Adaptive Control of M3C-Based Variable Speed Drive for Multiple PMSM-Driven Centrifugal Pumps

Rodrigo Mendoza-Becker , Juan Carlos Travieso-Torres * , Matías Díaz

Posted Date: 3 August 2023

doi: 10.20944/preprints202308.0302.v1

Keywords: M3C control; adaptive control; PMSM; model reference adaptive control; adaptive passivity-based control

Article

Adaptive Control of M3C-Based Variable Speed Drive for Multiple PMSM-Driven Centrifugal Pumps

Rodrigo Mendoza-Becker [1], Juan Carlos Travieso-Torres [2]* and Matías Díaz [1]

[1] Electrical Engineering Department, University of Santiago of Chile, Avenida Ecuador 3519; rodrigo.mendoza.b@usach.cl and matias.diazd@usach.cl
[2] Industrial Technologies Department, University of Santiago of Chile, El Belloto 3735; juancarlos.travieso@usach.cl
* Correspondence: juancarlos.travieso@usach.cl; Tel.: +569 5629 2048

Abstract: There has been growing interest in using permanent magnet synchronous motors (PMSMs) for pumping applications to improve energy efficiency. One promising approach for powering these motors in variable speed applications is using modular multilevel cascaded converters based on a Triple-Star Bridge Cell (M3C) due to their inherent fault tolerance capability. However, M3C converters require a more complex control system than simpler converters. For instance, A basic M3C control system for power transmission requires seventeen (17) PI controllers, whose adjustment depends on the M3C's dynamical model parameters' value knowledge needing extensive and time-consuming testing to obtain them. To solve this control system issue, we propose an adaptive M3C control system for variable speed drives powering multiple PMSM-driven centrifugal pumps that reduces the number of controllers to six (6). Furthermore, the proposal does not require knowledge of the converter, motor, or load parameters, making it more practical and versatile. The proposal introduces an ad-hoc hybrid passivity-based model reference adaptive controller in cascade with a passivity-based control. It has been validated through theoretical stability proof and comparative simulation results with a basic control system under normal and fault operations. As a result, the proposal effectively follows the required rotor speed while enhancing performance by decreasing the current consumption and recovering from a 10% input phase imbalance, a cell short circuit, and an open cell.

Keywords: M3C control; adaptive control; PMSM; model reference adaptive control; adaptive passivity-based control

1. Introduction

In recent years, a growing emphasis has been on utilizing permanent magnet synchronous motors (PMSM) to enhance energy efficiency in pumping applications [1]. Compared to traditional induction motors (IM), PMSM motors have demonstrated superior efficiency, as evidenced by [1, Figure 3]. The work [2] proposes customizing PMSM design for this application, while [3,4] study a variable speed PMSM for water pumps powered by AC-AC converter fed by photovoltaic panels. The works [3,4] use a two-level voltage source inverter controlled by model reference adaptive control (MRAC).

However, the work [5] proposes several fault-tolerant multilevel converters. In this sense, the use of modular multilevel cascaded converter (MMCC) obtained popularity due to its many benefits, such as redundancy, high efficiency, robustness, lower output voltage TDH, and low maintenance [6–8]. Among these converters, the triple-star bridge cells (M3C) topology is particularly noteworthy. M3C employs smaller floating capacitors [6,9].

What sets M3C apart is its inherent fault tolerance characteristics, allowing it to continue proper operations even after having a power supply phase imbalance or a power cell failure [6,9]. It ensures energy balancing with low impact on the output currents [9]. Furthermore, it reduces current harmonics, enhances power factor and efficiency, [6,8,10], eliminates voltage fluctuations and ensures optimal operation at low output frequencies [11,12]. There are even several studies that propose fault

Preprints (www.preprints.org) | NOT PEER-REVIEWED | Posted: 3 August 2023 doi:10.20944/preprints202308.0302.v1

detection and control under fault of M3C [13–15]. This manuscript focuses on controlling fault-tolerant M3C-based variable speed drive for PMSM-driven centrifugal pumps.

Figure 1 shows a commonly used M3C. It has modularity, the ability to reach high-voltage levels, power quality, bidirectional power conversion, and redundancy [16,17]. It has nine clusters (three per phase) that link the input phases (a, b, c) with the output phases (r, s, t), each consisting of three cells. Additionally, each cell has a full-bridge monophasic inverter. It has been widely utilized [18]; examples are to inject wind energy into an electrical network [17,19], and feed general loads [20].

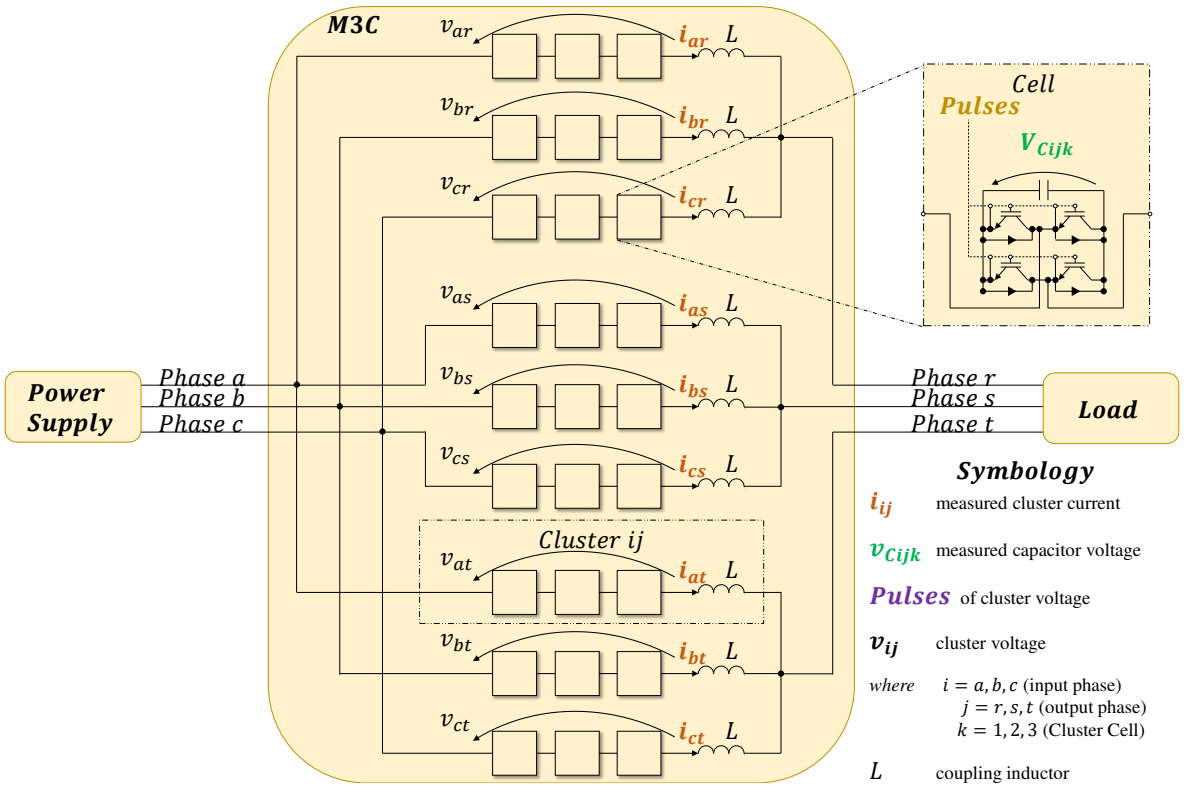

Figure 1. Basic power topology of an M3C for transferring energy between the power supply and the load, which is based on [6,9,19,21,22].

However, while having these fault-tolerant capabilities, controlling M3C is complex compared to simpler converters. Figure 2 describes how the control system of an M3C involves:

- Complex managing feedback signals that rearrange nine-dimensional measurement vectors i_{ij}, V_{Cij}, into matrixes form to work with variables at the intricate coordinate system called $2\alpha\beta\gamma$, and later rearrange them back to their vector form to allow the control [9,22,23].
- Controlling the average capacitor voltage (ACV) V_{Cavg} in cascade with the input currents amplitude I_{in} control, through the required input voltage v^*_{in-cl}.
- Keeping zero imbalance of the cluster capacitor voltage (CCV) in cascade with the circulating current i_{cir} control via the needed cluster voltage v^*_{cl}. It considers reducing to zero the Inter-CCV imbalances (CCV imbalance among clusters of different Sub-Converters) and the Intra-CCV imbalances (CCV imbalance among clusters inside the same Sub-Converters).
- Controlling a required output variable by adjusting the output voltage v^*_{out-cl} amplitude and frequency.

The control diagram of Figure 2 uses Park transform P [24], $\alpha\beta\gamma$ transform $\mathcal{C}$ [22], doble $\alpha\beta\gamma$ transform $\mathcal{C}X\mathcal{C}^T$ of different matrix variables X [22], and the combined components transformation matrix C_D [25]. Furthermore, the local cell balancing (LCB) and modulation block may use a phase-shifted (PS) pulse-wide modulation (PWM) technique [12,26], a space vector modulation (SVM)

Preprints (www.preprints.org) | NOT PEER-REVIEWED | Posted: 3 August 2023 doi:10.20944/preprints202308.0302.v1

[27] or Predictive Control [11,21]. This manuscript controls an M3C with the most extensively used PS-PWM [6].

Regarding the controllers, the works [17,21,25,28,29] consider M3C has several single-input and single-output (SISO) subsystems and use Proportional Integer (PI) controllers for all variables except for the circulating current. Most reported control strategies for the circulating current regulation are based on a simple P controller [17,25,28]. However, some authors use a P-resonant (PR) controller [21,29] as described in [6]. As a result, there are thirteen (13) PI controllers and four (4) PR or P controllers. One (1) PI regulates the ACV direct component in cascade with two (2) PIs for the input current amplitude direct and quadrature components. Eight (8) PIs aim to reduce the CCV imbalance in cascade with four (4) PR or P circulating current controllers. Finally, two (2) PIs regulate the load output current amplitude direct and quadrature components for energy transfer applications between the power supply and the load [6].

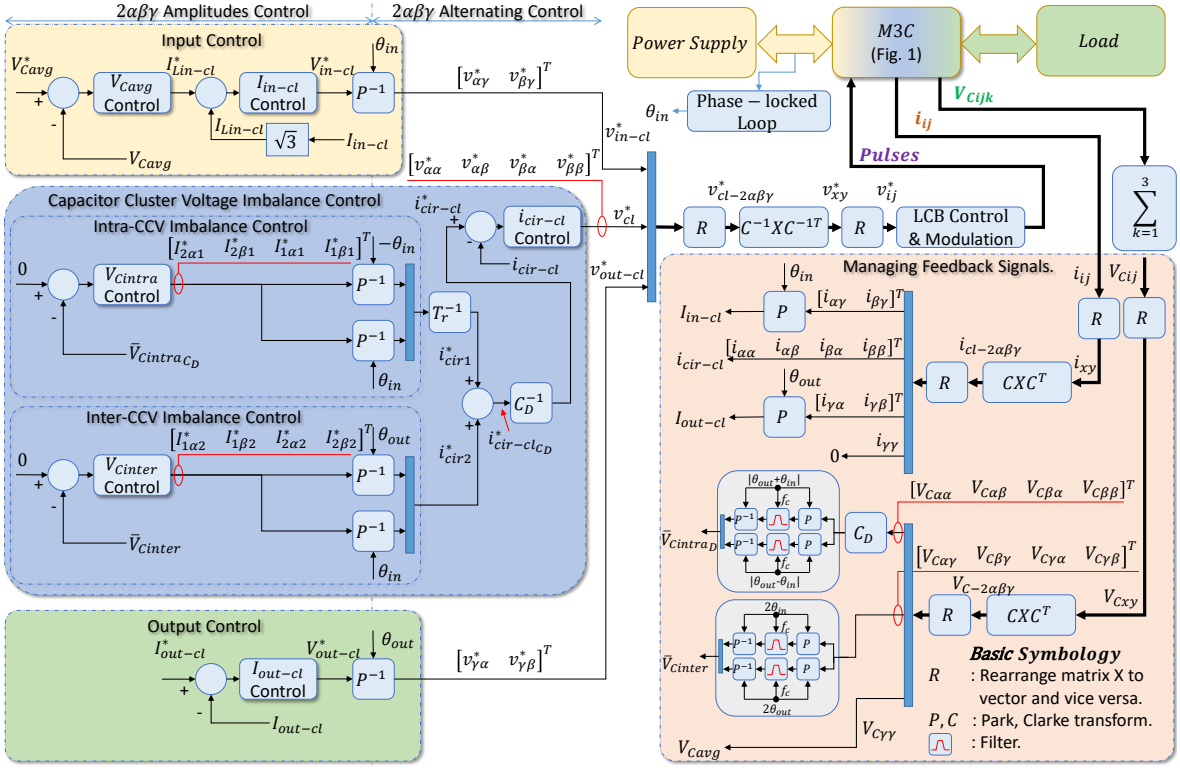

Figure 2. Basic control system of an M3C for transferring energy between the power supply and the load, which is based on [6,17,22,29].

The M3C has also been powering electrical motors with an output control strategy that differs from the one shown in Figure 2 and uses a speed control loop. The works [12,22,30] power IMs with an M3C, while [26] drives PMSMs. However, [12,22,26,30] do not describe the used output control strategy. In contrast, [31, Figure 3 (a)] clearly identifies a field-oriented control (FOC) strategy for an MMCC converter feeding IMs. Moreover, it presents multiple-input and multiple-output (MIMO) controllers, significantly reducing the number of controllers. All control systems proposed in [12,22,26,30,31] require knowledge of the plant parameters for their adjustment, which is typically obtained through extensive and time-consuming testing.

To overcome this issue and as the main contribution, this manuscript proposes a MIMO adaptive control of an M3C-based variable speed drive. It operates multiple PMSM-driven centrifugal pumps using a scalar control scheme (V/f) [32] for the output control, as FOC is unnecessary in pumping applications. Our proposal involves the following novelties:

Preprints (www.preprints.org) | NOT PEER-REVIEWED | Posted: 3 August 2023 doi:10.20944/preprints202308.0302.v1

1. **Obtaining the multivariable M3C state-space model for control.** It is a MIMO dynamical system with a currents inner loop, a voltages outer loop, and an inner-outer interface. Appendix A of this manuscript details the model obtaining, which complements, describes, rearranges, and summarizes elements taken from [6,22,23,33]. In contrast to [6,22,23,33], herein we give details for control implementation, such as the matrix and vector operations (please see, for instance, the Managing feedback signals details given in Figure 2), and identify the state-space model form with inner and outer loops.
2. **Using MIMO adaptive controllers instead of non-adaptive SISO controllers [17,21,25,28,29,31].** We show it is a viable and more straightforward solution. The proposal gains the benefits discussed in [31] of reducing the number of controllers by using a MIMO approach for an MMCC but herein for the M3C. In contrast to the works [17,21,25,28,29,31], tuning adaptive controllers does not require plant parameters knowledge, decreasing the commissioning time. Moreover, they adapt to plant changes without compromising their effectiveness.
3. **Proposing a passivity-based hybrid MRAC called PBMRAC.** In contrast to [3,4,34], it uses the MRAC as a low-pass filter for the noisy reference input signals. Moreover, PBMRAC introduces to MRAC a term of an adaptive passivity-based controller (APBC) [35] to attend to the closed-loop system response time. M3C control particularly needs it after having inner reference input noise periods more than sixty times distant from the M3C inner time constant.
4. **Presenting APBC in cascade with PBMRAC.** It expands the Cascade MRAC [36] and the cascade APBC [37]. The first uses an outer SISO controller, whereas the M3C outer loop requires a MIMO controller. Moreover, as Figure 2 shows, the M3C has zero or constant outer references eliminating the need for the outer reference model; therefore, an outer APBC [37] ensures a faster outer loop's time response.

The following manuscript sections describe the control preliminaries in Section 2. Section 3 details the proposed adaptive control algorithm. Section 4 exhibits the experimental setup and obtained results illustrating the proposal's effectiveness. Finally, the Authors present concluding remarks in Section 5.

2. Preliminaries

This section commences by introducing the M3C state-space dynamical model. Subsequently, it presents the conventional PI tuning methods. Finally, it gives the requisite background information of the cascade MRAC to be extended with the proposal.

2.1. M3C State-Space Model

The M3C state-space model obtaining is detailed in Appendix A, resulting in the equations (A7) and (A13). The following dynamical equations describe it:

$2\alpha\beta\gamma$ **Currents Inner Loop**

$$\begin{aligned} \dot{I_{Lin-cl}}(t) &= -\tfrac{\sqrt{3}}{L} V_{in-cl}(t) + \Delta_{in-cl}(t), && \text{Input current amplitude} \\ \dot{i_{cir-cl}}(t) &= -\tfrac{1}{L} v_{cl}(t), && \text{Circulating alternating current} \\ \dot{I_{out-cl}}(t) &= -\tfrac{1}{L} V_{out-cl}(t) + \Delta_{out-cl}(t), && \text{Output current amplitude} \end{aligned} \tag{1}$$

$2\alpha\beta\gamma$ **Inner-Outer Interface**

$$\begin{aligned} I_{Lin-cl}(t) &= [I_{Lin-cl\_d}(t) \quad 0]^T, \\ i_{cir-cl}(t) &= C_D^{-1} \left\{ T_r^{-1} \begin{bmatrix} P(-\theta_{in})^{-1} \\ P(\theta_{in})^{-1} \end{bmatrix} I_{cir1}(t) + \begin{bmatrix} P(-\theta_{out})^{-1} \\ P(\theta_{in})^{-1} \end{bmatrix} I_{cir2}(t) \right\}, \end{aligned} \tag{2}$$

Preprints (www.preprints.org) | NOT PEER-REVIEWED | Posted: 3 August 2023 doi:10.20944/preprints202308.0302.v1

$2\alpha\beta\gamma$ Voltages Outer Loop

$$\begin{aligned}
\dot{V}_{Cavg}(t) &= \frac{V_{avg}(t)}{3C\epsilon(t)V_C^*} I_{Lin-cl_d}(t) + \Delta_{avg}(t), && \text{ACV amplitude} \\
\dot{V}_{Cintra}(t) &= \frac{V_{intra}(t)^T}{\sqrt{6}C\epsilon(t)V_C^*} T_r I_{cir1}(t) + \Delta_{intra_{C_D}}(t), && \text{Intra-CCV imbalance amplitude} \\
\dot{V}_{Cinter}(t) &= \frac{V_{inter}(t)^T(t)}{\sqrt{3}C\epsilon(t)V_C^*} I_{cir2}(t) + \Delta_{inter}(t), && \text{Inter-CCV imbalance amplitude}
\end{aligned} \tag{3}$$

where in the inner loop, the output variables to control are the amplitudes of the input and output cluster currents $I_{in-cl} \in \Re^{2\times1}$ and $I_{out-cl} \in \Re^{2\times1}$, and the instantaneous circulating current $i_{cir-cl} \in \Re^{4\times1}$. Here, the input variables are the amplitudes of the input and output voltages $V_{in-cl} \in \Re^{2\times1}$ and $V_{out-cl} \in \Re^{2\times1}$, and the instantaneous cluster voltage $v_{cl} \in \Re^{4\times1}$. The parameter is the coupling inductors inductance L. Finally, the time-varying and bounded disturbance terms for the input are $\Delta_{in-cl}(t) = \frac{3}{L}\epsilon_{in}(t)V_{in\_rated} \in \Re^{2\times1}$ and $\Delta_{out-cl}(t) = -\frac{\sqrt{3}}{L}\epsilon_{out}(t)V_{out\_rated} \in \Re^{2\times1}$ for the output currents, where $\epsilon_{in}(t)$ and $\epsilon_{out}(t)$ are rated voltages fluctuations.

For the outer loop, the output variables are the ACV $V_{Cavg} \in \Re$, the intra-CCV imbalance $V_{Cintra} \in \Re^{4\times1}$, and the inter-CCV imbalance $V_{Cinter} \in \Re^{4\times1}$. The input variables are the amplitudes of the cluster input direct component $I_{in-cl\_d} \in \Re$, and the circulating currents $I_{cir1} \in \Re^{4\times1}$ and $I_{cir2} \in \Re^{4\times1}$. There are also time-varying bounded disturbance terms $\Delta_{avg}(t) \in \Re$, $\Delta_{intra_{C_D}}(t) \in \Re^{4\times1}$, and $\Delta_{inter}(t) \in \Re^{4\times1}$. Finally, the fixed parameters are the cells capacitor capacitance C and required capacitor voltage $V_C^* \in \Re$; while the time-varying parameters are the cluster voltages amplitudes $V_{intra}(t) \in \Re^{4\times1}$, $V_{inter}(t) \in \Re^{4\times1}$, $V_{avg}(t) \in \Re$, and the capacitor voltage fluctuations $\epsilon(t)$.

The inner-outer interface links the direct component of the line input cluster current I_{Lin-cl_d} with the input cluster current I_{in-cl}. Moreover, it relates the circulating current amplitudes I_{cir1} and I_{cir2} with the instantaneous circulating current i_{cir-cl}, after using the auxiliary transformation matrix C_D [25] and the Park transformation matrix P [24] with the corresponding input θ_{in} and output θ_{out} angles dependence. Please see Appendix A and Figure 2 for details.

Regarding the operating points in this $2\alpha\beta\gamma$ coordinate, the outer loops consider an ACV setpoint of $V_{Cavg}^* = 3V_C^*$ [22, Definition given bellow Equation (26)], working at zero intra-CCV Imbalance $V_{Cintra_{C_D}}^* = 0$ and zero inter-CCV Imbalance $V_{Cinter}^* = 0$ [18]. Moreover, the output current reference would be $I_{out-cl}^* = \frac{sqrt(3)}{3} I_{out}$ for applications of energy transference between the power supply and the load [6, Equation (24)].

The following section describes the PI controllers design for the M3C converter.

2.2. Basic Control Based PI Controllers

PI controllers design starts by assuming that plant parameters are constant, thus $\epsilon_{in}(t) = \epsilon_{out}(t) = \epsilon(t) = 1$. Later, the method splits every equation (1) to (3) in scalar subsystems having each one the general form $\dot{y}(t) = b \cdot u(t) + \delta(t)$. Here, $y(t) \in \Re$ is the output variable, $u(t) \in \Re$ is the input, b represents the fixed subsystems parameter, and $\delta(t)$ is the disturbance.

Then, Laplace transform is applied obtaining $Y(S) = (\frac{b}{S})(U(S) + b^{-1}\Delta(S)$, not including the circulating current working in alternating current. Here, the corresponding open-loop transfer function is $FT_{LA}(S) = \frac{b}{S}$, after neglecting the disturbance term, i.e., $\Delta(S) = 0$.

After considering the PI transfer function $(K_p + \frac{K_i}{S})$ acting in series with the FT_{LA}, the feed forward transfer function is $G(S) = (K_p + \frac{K_i}{S})(\frac{b}{S})$. Later, considering the feedback transfer function $H(S)$, you may obtain the following closed-loop transfer function as [38]:

$$FT_{LC} = \frac{G(S)}{1 + G(S)H(S)} = \frac{K_p b \cdot S + K_i b}{S^2 + K_p b \cdot S + K_i \cdot b} = \frac{2\xi\omega_n S + \omega_n^2}{S^2 + 2\xi\omega_n S + \omega_n^2}, \tag{4}$$

where ξ is the damping coefficient, and ω_n is the natural frequencies in rad/s.

Preprints (www.preprints.org) | NOT PEER-REVIEWED | Posted: 3 August 2023 doi:10.20944/preprints202308.0302.v1

The feedback sensor transfer function $H(S)$ is often considered a unitary gain. Moreover, we can identify in (4) the equivalence terms $2\xi\omega_n = K_p b$ and $\omega_n^2 = K_i b$, between the general second-order equation of the right side and the obtained result of the center side. It allows adjusting the PI controllers as follows:

$$K_p = \frac{2\xi\omega_n}{b}, \quad K_i = \frac{\omega_n^2}{b}. \tag{5}$$

To tune all PI controllers based on (5), $\xi = \frac{\sqrt{2}}{2}$ is usually considered [38, Section (5-3)]. However, there are different values of b, ω_n, and PI quantities for the distinct controlled variables, as Table 1 shows. Two (2) identical PI regulates the input and output current amplitude components d and q with $b = -\frac{\sqrt{3}}{L}$, as described in (1) and (A7). One (1) PI controls the ACV with $b = \frac{V_{avg}}{3CV_C^*}$ as can be seen in (3) and (A14). Four (4) PIs control the intra-CCV imbalance, where $V_{intra} = V_{in_\alpha}\begin{bmatrix}1 & 1 & 1 & 1\end{bmatrix}^T$ from (A14); thus, all components of the vector V_{intra} of are equal V_{in_α}, having the same $b = \frac{V_{intra}^T}{\sqrt{6}CV_C^*}$. Finally, also four (4) PI controls the inter-CCV imbalance. However, these have different values of b as described in Table 1, due to $V_{inter} = \begin{bmatrix}-V_{out_\alpha} & V_{out_\alpha} & V_{in_\alpha} & V_{in_\alpha}\end{bmatrix}^T$ from (A14).

Table 1. Values of b and ω_n for each controller.

Controller	b	ω_n	PI Quantity
Input Current Amplitude Control dq	$-\frac{\sqrt{3}}{L}$	$2\pi(f_{in})$	2
ACV Control d	$\frac{V_{avg}}{3CV_C^*}$	2π (1 Hz)	1
Intra-CCV Imbalance Control	$\frac{V_{in_\alpha}}{\sqrt{6}CV_C^*}$	2π (5 Hz)	4
Inter-CCV Imbalance Control $\alpha\gamma$	$-\frac{V_{out_\alpha}}{\sqrt{3}CV_C^*}$	2π (5 Hz)	1
Inter-CCV Imbalance Control $\beta\gamma$	$\frac{V_{out_\alpha}}{\sqrt{3}CV_C^*}$	2π (5 Hz)	1
Inter-CCV Imbalance Control $\gamma\alpha\beta$	$\frac{V_{in_\alpha}}{\sqrt{3}CV_C^*}$	2π (5 Hz)	2

The alternating circulating current controller often considers four (4) P controllers adjusted as in (5) but a $k_i = 0$ [23], and our case $b = -\frac{1}{L}$ and $\omega_n = 2\pi(10f_{out})$.

Finally, for applications of energy transference between the power supply and the load [6,17,22, 29], the output current amplitude control dq would have two PI controllers adjusted as in (5) and considering $b = -\frac{1}{L}$ and $\omega_n = 2\pi(f_{out})$.

Remark 1. *It is imperative to know the plant parameters value to adjust the PI controllers, as can be seen in equation (5) and Table 1. This knowledge is usually obtained through extensive testing, which can be time-consuming. It's also crucial for the controllers to handle plant changes without compromising their effectiveness.*

Preprints (www.preprints.org) | NOT PEER-REVIEWED | Posted: 3 August 2023 doi:10.20944/preprints202308.0302.v1

Finally, the output controller must be adjusted as we study pumping applications. Thus, the following P controller called scalar control scheme (V/f) is commonly used for a two-level voltage source inverter feeding PMSD-driven centrifugal pumps [32, Equation (1)]:

$$V^*_{out-cl\_d} = \begin{cases} 0 & \text{for } 0 < \omega_r < \omega_{r\_min} \\ P_1\omega^*_r + \sqrt{2}V_{boost}, \text{with } P_1 = \sqrt{2}(\frac{V_{s\_rated}}{\omega_{r\_rated}} - \frac{V_{boost}}{\omega_{r\_c}}) & \text{for } \omega_{r\_min} < \omega_r < \omega_{r\_c}. \\ P_2\omega^*_r, \text{with } P_2 = \sqrt{2}\frac{V_{s\_rated}}{\omega_{r\_rated}} & \text{for } \omega_{r\_c} < \omega_r < \omega_{r\_rated} \end{cases} \tag{6}$$

Here, V_{s_rated} is the rated phase voltage from the motor data plate. ω_{r_rated} is the motor-rated rotor speed in rad/s. The V_{boost} is a controller bias or offset (with a value up to 50% of V_{s_rated} allowing the PMSM to deliver a certain amount of starting torque. The V_{boost} operates from minimum frequency ω_{r_min} (with a value up to 6% of ω_{r_rated} to the cut-frequency ω_{r_c} (with a value up to 50% of ω_{r_rated}) [32].

Remark 2. *In order to attain the desired rotor angular frequency ω^*_r with a ramp-up, a two-level voltage source inverter necessitates a phase stator voltage amplitude of $V^*_{out-cl} = [V^*_{out-cl\_d} \quad 0]^T$. However, the output voltage required for the M3C is in double $\alpha\beta\gamma$ coordinates, utilizing a Power invariant transformation in lieu of Clarke's transformation that preserves the amplitude [39]. This paper proposes utilizing equation (6) [32, Equation (1)] in conjunction with the subsequent equation:*

$$V^*_{out-cl} = \sqrt{3}[V^*_{out-cl\_d} \quad 0]^T \tag{7}$$

The following section will give an overview of an adaptive controller that can maintain optimal performance while adapting to plant changes without requiring knowledge of plant parameters.

2.3. Cascade Adaptive Control Background

M3C modeled as (1) to (3) needs a cascade control system and the following cascade MRAC [36, Equations (14) - (22)] ensures the outputs y_o and y_i tracks the references y^*_o and y^*_i:

$$\begin{aligned} \dot{y}_{ro}(t) &= -a_{ro}y_{ro}(t) + b_{ro}y^*_o(t), && \text{Outer reference model} \\ u_o(t) &= -\theta_o(t)^T\omega_o(t), && \text{Outer adaptive control law} \\ \omega_o(t) &= \begin{bmatrix} y_o(t) & f_2(u;I,y_i) & y^*_o(t) \end{bmatrix}^T, && \text{MRAC outer information vector} \\ \dot{\theta}_o(t)^T &= -(sign(b_o)e_o(t)\omega_o(t)^T + \sigma_o\theta_o(t)^T)\Gamma_o, && \text{Outer adaptive law for MRAC} \\ \theta^*_o(t)^T &= \begin{bmatrix} b_o^{-1}(t)a_{ro} & b_o^{-1}(t)a_o & -b_o^{-1}(t)b_{ro} \end{bmatrix}, && \text{Ideal outer MRAC parameter} \end{aligned} \tag{8}$$

$$y^*_i(t) = f_1(u_o(t)), \quad \text{Inner-outer loop interface} \tag{9}$$

$$\begin{aligned} \dot{y}_{ri}(t) &= -A_{ri}y_{ri}(t) + B_{ri}y^*_i(t), && \text{Inner reference model} \\ u_i(t) &= -\theta_i(t)^T\omega_i(t), && \text{Inner adaptive control law} \\ \omega_i(t) &= \begin{bmatrix} y_i(t)^T & 1^T_m & y^*_i(t)^T \end{bmatrix}^T, && \text{MRAC inner information vector} \\ \dot{\theta}_i(t)^T &= -(sign(B_i)e_i(t)\omega_i(t)^T + \sigma_i\theta_i(t)^T)\Gamma_i, && \text{Inner adaptive law for MRAC} \\ \theta^*_i(t)^T &= \begin{bmatrix} B_i^{-1}A_{ri} & B_i^{-1}A_i(t) & -B_i^{-1}B_{ri} \end{bmatrix}. && \text{Ideal inner MRAC parameter} \end{aligned} \tag{10}$$

Here, the outer tracking error is $e_o(t) = y_{ro}(t) - y_o(t) \in \Re$ and the inner tracking error is $e_i(t) = y_{ri}(t) - y_i(t) \in \Re^m$. The variables $y_{ro}(t) \in \Re$, $y_{ri}(t) \in \Re^m$ are the outer and inner reference model outputs. The set point are $y^*_o(t) \in \Re$ and $y^*_i(t) \in \Re^m$. The reference model parameters are $a_{ro}, b_{ro} \in \Re$ and $A_{ri}, B_{ri} \in \Re^{(m\times m-Diagonal)}$ made equal ($a_{ro} = b_{ro}$ and $A_{ri} = B_{ri}$) for an exact set point tracking without scaling. The adaptive external and internal controllers $u_o(t) \in \Re$ and $u_i(t) \in \Re^m$ depends on their adaptive parameters $\theta_o(t) \in \Re^3$ and $\theta_i(t) \in \Re^{(m\times 3m)}$ and their corresponding information vectors $\omega_o(t) \in \Re^3$ and $\omega_i(t) \in \Re^{3m}$. The ideal adaptive parameters are $\theta^*_o(t) \in \Re^3$ and

Preprints (www.preprints.org) | NOT PEER-REVIEWED | Posted: 3 August 2023 doi:10.20944/preprints202308.0302.v1

$\theta_i^*(t) \in \Re^{(m\times 3m)}$. The term $1_m \in \Re^m$ refers to a vector with all its components equal to one. Besides the model reference parameters, the cascade MRAC has the following tuning parameters: adaptive law fixed-gains $\Gamma_o \in \Re^{(3\times 3-Diagonal)}$ and $\Gamma_i \in \Re^{(3m\times 3m-Diagonal)}$, and adaptive law modification factors $\sigma_o \in \Re$ and $\sigma_i \in \Re^{(3m\times 3m-Diagonal)}$.

Cascade MRAC (8)-(10) applies to time-varying cascade systems of the following form [36, Equations (11)-(13)]:

$$\begin{aligned} \dot{y}_i(t) &= A_i(t) + B_i(t)\cdot u_i(t), && \text{Inner loop} \\ y_i(t) &= f_1(u_o(t)), && \text{Inner-outer interface} \\ \dot{y}_0(t) &= a_o(t) f_2(u; I, y_i) + b_o(t)\cdot u_o(t), && \text{Outer loop} \end{aligned} \tag{11}$$

where $y_o(t) \in \Re$ and $y_i(t) \in \Re^m$ are the outer and inner output variables, respectively. The inputs are $u_o(t) \in \Re$ for the outer loop and $u_i(t) \in \Re^m$ for the inner loop. Moreover, $a_o(t), b_o(t) \in \Re$ and $A_i(t), B_i(t) \in \Re^{m\times m}$ are time-varying plant parameters, where $B_i(t) = |B_i(t)|Sign(B_i(t))$ and $b_0(t) = |b_0(t)|Sign(b_0(t))$ with $|B_i(t)|$ and $|b_0(t)|$ the modulus of each element of $B_i(t)$ and $b_0(t)$.

Remark 3. *It is important to note that the cascade MRAC (8)-(10) uses an outer SISO controller, whereas the M3C outer loop (3) requires a MIMO controller. Additionally, Figure 2 shows that M3C has zero or constant outer references, eliminating the need for the outer reference model of (8), which would slow down the outer loop's time response. Finally, the inner control loop receives noisy reference input signals with certain switching noise periods. Although the inner reference model of (10) could filter these signals, it would disregard the required inner loop response time, failing to ensure both needs.*

These issues are solved by the controller proposed in the following section.

3. Proposal

This section proposes an adaptive controller for the following system that encompasses the M3C state-space model (1)-(3):

$$\begin{aligned} \dot{y}_i(t) &= B_i(t)u_i(t) + \Delta_i(t), && \text{Inner loop} \\ y_i(t) &= f_1(u_o(t)), && \text{Inner-outer interface} \\ \dot{y}_0(t) &= B_o(t)u_o(t) + \Delta_o(t), && \text{Outer loop} \end{aligned} \tag{12}$$

where $y_o(t) \in \Re^n$ and $y_i(t) \in \Re^m$ are the outer and inner output variables, respectively. The outer control input is $u_o(t) \in \Re^n$ and the inner is $u_i(t) \in \Re^m$. Moreover, $B_o(t) \in \Re^{n\times n}$ and $B_i(t) \in \Re^{m\times m}$ are time-varying and unknown plant parameters, where $B_i(t) = |B_i(t)|Sign(B_i(t))$ and $B_0(t) = |B_0(t)|Sign(B_0(t))$. Here, the matrix $|B_i(t)|$ and $|B_0(t)|$ are compose by the modulus of each element of $B_i(t)$ and $B_0(t)$ and are unknown. Furthermore, the matrix $Sign(B_i(t))$ and $Sign(B_0(t))$ are compose by the sign of each element of $B_i(t)$ and $B_0(t)$ and are known. The known interface nonlinear function is $f_1 \in \Re^{m\times n}$. Finally, $\Delta_i(t)$ and $\Delta_o(t)$ are the inner and outer bounded and unknown disturbances, respectively.

The following Theorem describes the proposal:

Theorem 1. *For systems of the form (12), the following adaptive controller ensures the outputs y_o and y_i tends to the constant references y_o^* and y_i^*, respectively:*

$$\begin{aligned} u_o(t) &= -\theta_o(t)^T\omega_o(t), && \textit{Outer control law} \\ \omega_o(t) &= \left[\Delta_{o\_b}^T \quad u_o^p(t)^T\right]^T, \textit{ with } u_o^p(t) = K_o\nabla V_{e_o}(t), && \textit{APBC outer information vector} \\ \dot{\theta}_o(t)^T &= -(sign(b_o)\nabla V_{e_o}(t)\omega_o(t)^T + \sigma_o\theta_o(t)^T)\Gamma_o, && \textit{APBC outer adaptive law} \\ \theta_o^*(t)^T &= \left[B_o^{-1}(t) \quad B_o^{-1}(t)\right], && \textit{Ideal outer APBC parameter} \end{aligned} \tag{13}$$

Preprints (www.preprints.org) | NOT PEER-REVIEWED | Posted: 3 August 2023 doi:10.20944/preprints202308.0302.v1

$$y_i^*(t) = f_1(u_o(t)), \quad \textit{Inner-outer loop interface} \tag{14}$$

$$\begin{aligned}
&\dot{y}_{ri}(t) = -A_{ri}y_{ri}(t) + B_{ri}y_i^*(t), && \textit{Inner reference model}\\
&u_i(t) = -\theta_i(t)^T\omega_i(t), && \textit{Inner control law based}\\
&\omega_i(t) = \begin{bmatrix} y_i(t)^T & y_i^*(t)^T & \Delta_{i_b}^T & u_i^p(t)^T \end{bmatrix}^T, && \textit{PBMRAC inner inform. vector}\\
&\textit{with } u_i^p(t) = K_i\nabla V_{e_i}(t),\\
&\dot{\theta}_i(t)^T = -(sign(B_i)\nabla V_{e_i}(t)\omega_i(t)^T + \sigma_i\theta_i(t)^T)\Gamma_i, && \textit{PBMRAC inner adaptive law}\\
&\theta_i^*(t)^T = \begin{bmatrix} B_i^{-1}A_{ri} & -B_i^{-1}B_{ri} & B_i^{-1} \end{bmatrix}. && \textit{Ideal inner PBMRAC parameter}
\end{aligned} \tag{15}$$

Here, the outer tracking error is $e_o(t) = y_{ro}(t) - y_o(t) \in \Re^n$ and the inner tracking error is $e_i(t) = y_{ri}(t) - y_i(t) \in \Re^m$. The variables $y_{ro}(t) \in \Re^n$ and $y_{ri}(t) \in \Re^m$ are the outer and inner reference model outputs, respectively. The set points are $y_o^*(t) \in \Re^n$ and $y_i^*(t) \in \Re^m$. The inner and outer controllers $u_o(t) \in \Re^n$ and $u_i(t) \in \Re^m$ depends on their adaptive parameters $\theta_o(t) \in \Re^{n\times 2n}$ and $\theta_i(t) \in \Re^{(m\times 3m)}$ and their corresponding information vectors $\omega_o(t) \in \Re^{2n}$ and $\omega_i(t) \in \Re^{3m}$. The unknown ideal adaptive parameters are defined as $\theta_o^*(t) \in \Re^{n\times 2n}$ and $\theta_i^*(t) \in \Re^{(m\times 3m)}$. Moreover, $V_{e_o}(t)$ and $V_{e_i}(t)$ are Lyapunov-type energy terms.

Following, the adaptive controller tuning parameters settings are described. The outer APBC loop tunes the outer PB gain as $K_o = \frac{5\delta_{1o}}{T_s^*} I_n \in \Re^{(n\times n-Diagonal)}$, where $5T_s^*$ is the process required stabilization time [32]. The adaptive law modification term is $\sigma_o = \delta_{2o} I_n \in \Re^{(n\times n-Diagonal)}$, depending on the identity matrix I_n of order n. The adaptive law fixed-gain is $\Gamma_o \in \Re^{(2n\times 2n-Diagonal)}$. Moreover, the fine-tuning scalar factors are $0 < \alpha_{o1l}, \alpha_{o2l} < 10$ and $0 < \delta_{1o}, \delta_{2o} < 10$, with $l = 1, 2, 3, ..., n$ [36, Theorem 1]. Finally, APBC adjusts the adaptive law fixed-gain [32, Equation (11)] as follows:

$$\Gamma_o = Diag\left[\frac{\alpha_{o11}\Delta_{o1\_b}}{1+\Delta_{o1\_b}^2} \quad \cdots \quad \frac{\alpha_{o1n}\Delta_{on\_b}}{1+\Delta_{on\_b}^2} \quad \frac{\alpha_{o21}u_{o1\_b}^p}{1+u_{o1\_b}^{p\,2}} \quad \cdots \quad \frac{\alpha_{o2n}u_{on\_b}^p}{1+u_{on\_b}^{p\,2}}\right]. \tag{16}$$

The inner PBMRAC loop adjusts the model reference parameter as $A_{ri} = \frac{f_{noise}\delta_{1i}}{20} I_n \in \Re^{(n\times n-Diagonal)}$. The PB gain K_i is computed as $(A_{ri} + K_i) = 15K_o$ (over fifteen times faster than the outer loop), and the adaptive law modification terms $\sigma_i = \delta_{2i} I_m \in \Re^{(m\times m-Diagonal)}$. Here, $0 < \delta_{1i}, \delta_{2i} < 10$ are fine-tuning scalar adjusting factors, toguether with $0 < \alpha_{i1l}, \alpha_{i2l}, \alpha_{i3l}, \alpha_{i4l} < 10$ where $l = 1, 2, 3, ..., n$. Finally, the adaptive law fixed-gain $\Gamma_i \in \Re^{(2m\times 2m-Diagonal)}$ is adjusted via the following equation [36, Theorem 1]:

$$\begin{aligned}
\Gamma_i = Diag\Bigg[&\frac{\alpha_{i11}y_{i1_b}}{1+y_{i1_b}^2} \quad \cdots \quad \frac{\alpha_{i1n}y_{in_b}}{1+y_{in_b}^2} \quad \frac{\alpha_{i21}y_{i1_b}^*}{1+y_{i1_b}^{*\,2}} \quad \cdots \quad \frac{\alpha_{i2n}y_{in_b}^*}{1+y_{in_b}^{*\,2}}\\
&\frac{\alpha_{i31}\Delta_{i1_b}}{1+\Delta_{i1_b}^2} \quad \cdots \quad \frac{\alpha_{i3n}\Delta_{in_b}}{1+\Delta_{in_b}^2} \quad \frac{\alpha_{i41}u_{i1_b}^p}{1+u_{i1_b}^{p\,2}} \quad \cdots \quad \frac{\alpha_{i4n}u_{in_b}^p}{1+u_{in_b}^{p\,2}}\Bigg].
\end{aligned} \tag{17}$$

Following is the Theorem Proof.

Proof of Theorem 1. As a result of applying the adaptive controllers (13) and (15) to the corresponding dynamical equation of (11), we obtain the closed-loop dynamical error equations whose require verification of their stability.

In detail, the term $u_o^p(t)$ is added and subtracted to the right side of the outer loop equation of (11). The outer control law of (13) is then applied, the outer tracking error definition $e_o(t) = y_o^*(t) - y_i(t)$ considered, and the terms regrouped conveniently. In regards to the inner loop, we subtract the inner reference model of (15) from the inner loop equation of (11). Later, we add and subtract the term $A_{ri}y_i(t)$ to the right side and consider the inner tracking error definition $e_i(t) = y_{ri}(t) - y_i(t)$.

Preprints (www.preprints.org) | NOT PEER-REVIEWED | Posted: 3 August 2023 doi:10.20944/preprints202308.0302.v1

Moreover, we apply the inner control law of (15) and regroup terms. As a result, the following control error dynamical equations is obtained:

$$\begin{aligned} \dot{e}_o(t) &= u_o^p(t) - B_o(t)\phi_o(t)^T\omega_o(t), \\ \dot{e}_i(t) &= -A_{ri}e_i(t) + u_i^p(t) - B_i(t)\phi_i(t)^T\omega_i(t), \end{aligned} \tag{18}$$

where $\phi_o(t)^T = \theta_o(t)^T - \theta_o^*(t)^T$ and $\phi_i(t)^T = \theta_i(t)^T - \theta_i^*(t)^T$ are the adaptive parameters errors. Obtaining now the first-time derivative of $\phi_o(t)^T$ and $\phi_i(t)^T$, considering the definitions given in Theorem 1 for $\theta_o(t)^T$, $\theta_o^*(t)^T$, $\theta_i(t)^T$, and $\theta_i^*(t)^T$, these errors dynamical equations give:

$$\begin{aligned} \dot{\phi}_o(t)^T &= -(sign(B_o)\nabla V_{e_o}(t)\omega_o(t)^T + \sigma_o\theta_o(t)^T)\Gamma_o - \dot{\theta}_o^*(t)^T, \\ \dot{\phi}_i(t)^T &= -(sign(B_i)\nabla V_{e_i}(t)\omega_i(t)^T + \sigma_i\theta_i(t)^T)\Gamma_i - \dot{\theta}_i^*(t)^T. \end{aligned} \tag{19}$$

These closed-loop dynamical error equations (18) and (19) have the following associated Lyapunov function:

$$V(e_i, e_0, \phi_i, \phi_o) = V_{e_i} + V_{e_0} + Trace(\tfrac{1}{2}|B_i|\phi_i^T\Gamma_i^{-1}\phi_i) + \tfrac{1}{2}|b_o|\phi_o^T\Gamma_o^{-1}\phi_o. \tag{20}$$

Taking the first-time derivative of (20), considering the derivative property of the product in the trace, and replacing the control errors dynamical equations (18), we obtain:

$$\begin{aligned} \dot{V}(e_i, e_0, \phi_i, \phi_o) = &-\nabla V_{e_i}^T A_{ri}e_i - \nabla V_{e_i}^T u_i^p + \nabla V_{e_i}^T B_i\phi_i^T\omega_i - \nabla V_{e_o}^T u_o^p + \nabla V_{e_o}^T B_o\phi_o^T\omega_o \\ &+Trace(|B_i|\dot{\phi}_i^T\Gamma_i^{-1}\phi_i) + |B_o|\dot{\phi}_o^T\Gamma_o^{-1}\phi_o. \end{aligned} \tag{21}$$

Moreover, using the vector property $a^Tb = Trace(ab^T)$, we can rewrite the following term $(\nabla V_{e_o}^T B_o)(\phi_o^T\omega_o) = Trace((B_o^T\nabla V_{e_o})(\omega_o^T\phi_o))$. Moreover, we can also re express the term $(\nabla V_{e_i}^T B_i)(\phi_i^T\omega_i) = Trace((B_i^T\nabla V_{e_i})(\omega_i^T\phi_i))$. Finally, considering that $B_o = |B_o|Sign(B_0)$ and $B_i = B_i^T = |B_i(t)|Sign(B_i(t))$ (due to B_i is diagonal), it gives the following expression:

$$\begin{aligned} &\dot{V}(e_i, e_0, \phi_i, \phi_o) - \nabla V_{e_i}^T A_{ri}e_i - \nabla V_{e_i}^T u_i^p - \nabla V_{e_o}^T u_o^p \\ &+Trace(|B_i|sign(B_i)\nabla V_{e_i})(\omega_i^T\phi_i)) + |B_i|\dot{\phi}_i^T\Gamma_i^{-1}\phi_i) \\ &+Trace(|B_o|sign(B_o)\nabla V_{e_o})(\omega_o^T\phi_o)) + |B_o|\dot{\phi}_i^T\Gamma_o^{-1}\phi_o). \end{aligned} \tag{22}$$

Here, replacing the control parameters errors dynamical equation (19), canceling terms, and taking into account the expressions $\theta_o(t)^T = \phi_o(t)^T + \theta_o^*(t)^T$ and $\theta_i(t)^T = \phi_i(t)^T + \theta_i^*(t)^T$, the Lyapunov function first-time derivative becomes:

$$\begin{aligned} \dot{V}(e_i, e_0, \phi_i, \phi_o,) = &-\nabla V_{e_i}^T A_{ri}e_i - \nabla V_{e_i}^T u_i^p - \nabla V_{e_o}^T u_o^p \\ &-Trace(|B_i|\sigma_i\phi_i^T\phi_i) - Trace(|B_o|\sigma_o\phi_o^T\phi_o) \\ &-Trace(|B_i|\sigma_i{\theta_i^*}^T\phi_i) - Trace(|B_i|{\dot{\theta}_i^*}^T\Gamma_i^{-1} \\ &-Trace(|B_o|\sigma_o{\theta_o^*}^T\phi_o) - Trace(|B_o|{\dot{\theta}_o^*}^T\Gamma_o^{-1}. \end{aligned} \tag{23}$$

Here, we have that A_{ri}, $|B_i|$, σ_i, $|B_o|$, and σ_o are positives; therefore the first five terms of (23) are negatives. However, although the terms Γ_i and Γ_o are also positives, there is nothing we can say about the sign of the last fourth terms of (23) at first sight. Therefore, we re-express equation (23) using some modulus and norm properties.

Using the Frobenius norm definition and the Cauchy–Schwarz inequality, we have that $|Trace(ABC)| \leq \|A\|_F\|B\|_F\|C\|_F$ [40, Section 11.2.2]. Moreover, considering a positive A, $Trace(AB^TB) = |Trace(AB^TB)| \leq \|A\|_F\|B\|_F^2$. Therefore, the following terms become $-Trace((|B_i|\sigma_i)\phi_i^T\phi_i) \leq -\|(|B_i|\sigma_i)\|_F\|\phi_i\|_F^2$ and $-Trace((|B_o|\sigma_o)\phi_o^T\phi_o) \leq -\|(|B_o|\sigma_o)\|_F$ $\|\phi_o\|_F^2$. Also, the last fourth terms fulfill $-Trace(|B_i|\sigma_i{\theta_i^*}^T\phi_i) \leq -\|(|B_i|\sigma_i)\|_F\|{\theta_i^*}^T\|_F\|\phi_i\|_F$, $-Trace(|B_o|\sigma_o{\theta_o^*}^T\phi_o) \leq -\|(|B_o|\sigma_o)\|_F\|{\theta_o^*}^T\|_F\|\phi_o\|_F$, $-Trace(|B_i|{\dot{\theta}_i^*}^T\Gamma_i^{-1}\phi_i) \leq -\|(|B_i|)\|_F$ $\|\dot{\theta}_i^*\|_F\|\phi_i\|_F\|\Gamma_i^{-1}\|_F$, and $-Trace(|B_o|{\dot{\theta}_o^*}^T\Gamma_o^{-1}\phi_o) \leq -\|(|B_o|)\|_F\|\dot{\theta}_o^*\|_F\|\phi_o\|_F\|\Gamma_o^{-1}\|_F$. Finally, using the

Preprints (www.preprints.org) | NOT PEER-REVIEWED | Posted: 3 August 2023 doi:10.20944/preprints202308.0302.v1

property $2ab \leq a^2 + b^2$ [40, Section 11.2.2], and conveniently adding the term r^2 to the right side of equation (23), the Lyapunov function first-time derivative (23) becomes:

$$\begin{array}{c}\dot{V}(e_i, e_0, \phi_i, \phi_o,) = -\nabla V_{e_i}^T A_{ri} e_i - \nabla V_{e_i}^T u_i^p - \nabla V_{e_o}^T u_o^p \\ +r^2 - \|(|B_i|\sigma_i)\|_F \|\phi_i\|_F^2 \quad - \|(|B_o|\sigma_o)\|_F \|\phi_o\|_F^2 \\ -\frac{1}{2}\|(|B_i|\sigma_i)\|_F \|(\theta_i^{*^T}\|_F^2 + \|\phi_i\|_F^2) - \frac{1}{2}\|(|B_o|\sigma_o)\|_F \|(\theta_o^{*^T}\|_F^2 + \|\phi_o\|_F^2) \\ -\frac{1}{2}\|(|B_i|)\|_F (\|\dot{\theta}_i^*\|_F^2 + \|\phi_i\|_F^2)\|\Gamma_i^{-1}\|_F - \frac{1}{2}\|(|B_o|)\|_F (\|\dot{\theta}_o^*\|_F^2 + \|\phi_o\|_F^2)\|\Gamma_o^{-1}\|_F,\end{array} \tag{24}$$

where the plant parameters and their first-time derivatives are bounded. Therefore, $\dot{V} \leq -\nabla V_{e_i}^T u_i^p - \nabla V_{e_o}^T u_o^p$ and closed-loop dynamical error equations (18) and (19) are passive outside the region Ω. This last, is the following instability hyper elliptical paraboloid that is compact, closed, and includes the origin:

$$\begin{array}{c}\Omega = [\|(|B_i|\sigma_i)\|_F \|\phi_i\|_F^2 \quad + \|(|B_o|\sigma_o)\|_F \|\phi_o\|_F^2 \\ +\frac{1}{2}\|(|B_i|\sigma_i)\|_F \|(\theta_i^{*^T}\|_F^2 + \|\phi_i\|_F^2) + \frac{1}{2}\|(|B_o|\sigma_o)\|_F \|(\theta_o^{*^T}\|_F^2 + \|\phi_o\|_F^2) \\ +\frac{1}{2}\|(|B_i|)\|_F (\|\dot{\theta}_i^*\|_F^2 + \|\phi_i\|_F^2)\|\Gamma_i^{-1}\|_F + \frac{1}{2}\|(|B_o|)\|_F (\|\dot{\theta}_o^*\|_F^2 + \|\phi_o\|_F^2)\|\Gamma_o^{-1}\|_F] < r^2.\end{array} \tag{25}$$

Furthermore, substituting into (25), the terms $u_o^p(t) = K_o \nabla V_{e_o}(t)$ and $u_i^p(t) = K_i \nabla V_{e_i}(t)$ defined in (13) and (15), and using Lyapunov's second method, we can conclude that the closed-loop dynamical error equations (18) and (19) are bounded outside Ω. Suppose the errors are as minor as possible, resulting in $\dot{V} > 0$ within the instability compact and closed region Ω, including the origin. In that case, they will be pushed back to a stable boundary. In practice, the values of $\sigma_i, \sigma_o, \Gamma_i$, and Γ_o are chosen so the permanent errors are the possible lowest.

Thus, $e_i(t), e_o(t), \phi_i(t)$, and $\phi_o(t)$ are bounded outside Ω, i.e., $e_i(t), e_o(t), \phi_i(t), \phi_o(t) \in L^\infty$ outside Ω. Since $e_i(t) = y_i(t) - y_{ri}$ and $e_o(t) = y_o(t) - y_{ro}$ are bounded, it implies that $y_i(t)$ and $y_o(t)$ are bounded, as y_{ri}, y_i^* and y_{ro}, y_0^* are bounded references. Moreover, $\phi_i(t)$ and $\phi_o(t)$ are bounded, and we have bounded plant parameters, then the adaptive parameters $\theta_i(t)$ and $\theta_o(t)$ are bounded, since $\theta_i(t)^T = \phi_i(t)^T + \theta_i^*(t)^T$ and $\theta_o(t)^T = \phi_o(t)^T + \theta_o^*(t)^T$. Having all these bounded signals outside Ω, and that $V, e(t), \phi(t) \in L^\infty$, from (18) and (19), we have that $\dot{e}_i(t), \dot{e}_o(t), \dot{\phi}_i(t), \dot{\phi}_o(t) \in L^\infty$. Integrating both sides of $\dot{V}(e_i, e_0, \phi_i, \phi_o,)$ in the interval $(0, \infty)$, it gives

$$\begin{array}{c}V(\infty) - V(0) = \int_0^\infty (-\nabla V_{e_i}^T A_{ri} e_i - \nabla V_{e_i}^T K_i \nabla V_{e_i}(t) - \nabla V_{e_o}^T K_o \nabla V_{e_o}(t) \\ +r^2 - \|(|B_i|\sigma_i)\|_F \|\phi_i\|_F^2 \quad - \|(|B_o|\sigma_o)\|_F \|\phi_o\|_F^2 \\ -\frac{1}{2}\|(|B_i|\sigma_i)\|_F \|(\theta_i^{*^T}\|_F^2 + \|\phi_i\|_F^2) - \frac{1}{2}\|(|B_o|\sigma_o)\|_F \|(\theta_o^{*^T}\|_F^2 + \|\phi_o\|_F^2) \\ -\frac{1}{2}\|(|B_i|)\|_F (\|\dot{\theta}_i^*\|_F^2 + \|\phi_i\|_F^2)\|\Gamma_i^{-1}\|_F - \frac{1}{2}\|(|B_o|)\|_F (\|\dot{\theta}_o^*\|_F^2 + \|\phi_o\|_F^2)\|\Gamma_o^{-1}\|_F)\, d\tau.\end{array} \tag{26}$$

As V is bounded outside Ω, from the right-hand side of this last equation; we have that $e(t) \in L^2$ outside Ω. Furthermore, as $e_i(t), \dot{e}_i(t) \in L^\infty$ and $e_i(t) \in L^2$, and $e_o(t), \dot{e}_o(t) \in L^\infty$ and $e_0(t) \in L^2$, all outside Ω, using Barbalat's Lemma [34, Section 4.5.2] we have that $e_i(t)$ and $e_o(t)$, both tend asymptotically to zero outside Ω. Hence, $y_i(t) \to y_i^*$ and $y_o(t) \to y_o^*$ outside Ω^c. We do not ensure parameter convergence. This concludes the proof. □

The following section applies the proposed controller to the M3C converter and describes the obtained results.

4. Simulation Results

This section applies the proposed control system shown in Figure 2 to the power topology of Figure 1 with three cells per cluster. It runs on a personal computer, in PLECS 4.7.2. The modeling settings are solver RADAU with variable-step, using a relative tolerance of 1×10^{-3}.

The M3C load corresponds to four equal PMSMs electrically connected in parallel and moving a centrifugal pump each. Table 2 shows the motor-pump parameters.

Preprints (www.preprints.org) | NOT PEER-REVIEWED | Posted: 3 August 2023 doi:10.20944/preprints202308.0302.v1

Table 2. Motor-pump parameters.

Parameter	Value	Parameter	Value
P_{rated}	644 [W]	T_{rated}	4.1 [N-m]
V_{s_rated}	165 [V]	I_{s_rated}	2.65 [A]
f_e	75 [Hz]	f_p	0.95
P	3	Φ	0.305 [Wb]
ω_r	157.08[rad/s]	J_m	0.0036 [Nms^2]
R_s	6.2 [Ω]	J_{Load}	0.0108 [Nms^2]
L_d	25.025 [mH]	K_{load}	93.053 $\cdot 10^{-6}$ [Kg m^2]
L_q	40.17 [mH]	T_0	0.41 [N-m]

Here, V_{s_rated} and I_{s_rated} are the rated stator voltage and current of the PMSM, respectively. The power factor is f_p and f_e is the electric required frequency of the PMSM for it to run at rated speed. P is the number of pole pairs and ω_r is the PMSM rated speed. The PMSM-rated torque and power are T_{rated} and P_{rated}, respectively. Moreover, R_s, L_d and L_q are the resistance and inductance of the motor, Φ is the magnetic flux induced by the motor magnets, J_m is the motor inertia, J_{Load} is the inertia of the load. On the other hand, the load parameters are the initial load torque T_0 are zero speed and the constant K_{load}, characterizing the pump model equation $T_{Load} = K_{load} \cdot \omega_r^2 + T_0$.

The M3C is designed to power these PMSMs-driven centrifugal pumps, having the same P_{rated}. Table 3 presents the plate data and parameters value of the M3C.

Table 3. Plate data and parameters value of the M3C.

Parameter	Value	Parameter	Value
P_{rated}	644 [W]	V_C^*	1500 [V]
V_{in_rated}	220 [V]	V_{out_rated}	165 [V]
f_{in}	50 [Hz]	f_{out}	75 [Hz]
L_{in}	1.5 [mH]	L	1.0 [mH]
f_{sw}	10 [KHz]	C	3.3 [mF]

The reference capacitor voltage mean value V_C^* is defined based on the M3C input and output rated voltages V_{in_rated} and V_{out_rated} and the number of cells. Here, $V_C^* \geq 1.2 \cdot \sqrt{2} \cdot (V_{in\_rated} + V_{out\_rated})$, been divisible by 3 (number of cells per cluster). Therefore, $V_C^* \geq 1.2 \cdot \sqrt{2} \cdot (V_{in\_rated} + V_{out\_rated}) = 3 \cdot 500[V] = 1500[V] \geq 1.2\sqrt{2} \cdot (220[V] + 400[V]) \geq 1052[V]$.

Moreover, the Power supply has the rated voltage V_{in_rated}, the input frequency f_{in}, and an input inductance L_{in}. The load has the rated voltage V_{out_rated} equals the rated motor voltage V_s_rated, and an output frequency f_{out} equals rated motor frequency f_e. Finally, we have the cells with switching frequency f_{sw} and a capacitance capacitor C. The cluster coupling inductance is L.

The following two control systems are applied to the M3C-based variable speed drive for multiple PMSM-driven centrifugal pumps for comparison purposes:

Basic Control System [23].

The basic control includes sixteen (16) PI controllers, whose settings are calculated based on the definitions provided in equation (5) and Table 1:

- Input Control:
  - One (1) PIs for the $2\alpha\beta\gamma$ ACV Control:

$$K_p\_V_{Cavg} = \frac{8.485\pi CV_C^*}{V_{avg}} = 0.4241, \quad K_i\_V_{Cavg} = \frac{12\pi^2 CV_C^*}{V_{avg}} = 1.8843,$$

Preprints (www.preprints.org) | NOT PEER-REVIEWED | Posted: 3 August 2023 doi:10.20944/preprints202308.0302.v1

where the constant cluster voltage amplitude is $V_{avg} = V_{in_d} = \sqrt{2}V_{in\_rated}$. The output of the ACV controller is the input cluster line current amplitude direct component reference $I^*_{Lin-cl\_d}$. Here, the input cluster line current amplitude reference is $I^*_{Lin-cl} = [I_{Lin-cl\_d} \quad 0]^T$ and is controlled by the following controllers.

- Two (2) PIs for the $2\alpha\beta\gamma$ input cluster line current I_{Lin-cl} amplitude direct and quadrature components:

$$K_p\_I_{in-cl\_d} = K_p\_I_{in-cl\_q} = -\frac{\sqrt{2}(2\pi f_{in})L}{\sqrt{3}} = -81.65\pi L = -0.2567,$$
$$K_i\_I_{in-cl\_d} = K_i\_I_{in-cl\_q} = -\frac{(2\pi f_{in})^2 L}{\sqrt{3}} = -5773.5\pi^2 L = -56.98.$$

- CCV Imbalance Control.
  - Four (4) PIs for the $2\alpha\beta\gamma$ Intra-CCV Imbalance Control [23, Outer controller of Figure 3]:

$$K_p\_V_{C1\alpha} = K_p\_V_{C1\beta} = K_p\_V_{C2\alpha} = K_p\_V_{C2\beta} = \frac{14.142\pi\sqrt{6}CV^*_C}{V_{in_d}} = 1.1541,$$
$$K_i\_V_{C1\alpha} = K_i\_V_{C1\beta} = K_i\_V_{C2\alpha} = K_i\_V_{C2\beta} = \frac{100\pi^2\sqrt{6}CV^*_C}{V_{in_d}} = 25.642.$$

  - Four (4) PIs for the $2\alpha\beta\gamma$ Inter-CCV Imbalance Control [23, Figure 4]:

$$K_p\_V_{C\alpha\gamma} = -\frac{14.142\pi\sqrt{3}CV^*_C}{V_{out_d}} = -0.6348, \quad K_p\_V_{C\beta\gamma} = \frac{14.142\pi\sqrt{3}CV^*_C}{V_{out_d}} = 0.6348,$$
$$K_p\_V_{C\gamma\alpha} = K_p\_V_{C\gamma\beta} = \frac{14.142\pi\sqrt{3}CV^*_C}{V_{in_d}} = 0.8161,$$
$$K_i\_V_{C\alpha\gamma} = -\frac{100\pi^2\sqrt{3}CV^*_C}{V_{out_d}} = -14.1031, \quad K_i\_V_{C\beta\gamma} = \frac{100\pi^2\sqrt{3}CV^*_C}{V_{out_d}} = 14.1031,$$
$$K_i\_V_{C\gamma\alpha} = K_i\_V_{C\gamma\beta} = \frac{100\pi^2\sqrt{3}CV^*_C}{V_{in_d}} = 18.1316,$$

with the constant voltage $V_{out_d} = \sqrt{2}V_{out\_rated}$. Both of these controllers are in cascade with the following controller:

  - Four (4) PIs controllers for the $2\alpha\beta\gamma$ circulating current, considering only a P action [23, Inner controller of Figure 3]:

$$K_p\_i_{circ-cl\_\alpha\alpha} = K_p\_i_{circ-cl\_\alpha\beta} = K_p\_i_{circ-cl\_\beta\alpha} = K_p\_i_{circ-cl\_\beta\beta}$$
$$= -\sqrt{2}\sqrt{3}(2\pi 10 f_{out}) = -4242,64\pi L = -13.3266,$$
$$K_i\_i_{circ-cl\_\alpha\alpha} = K_i\_i_{circ-cl\_\alpha\beta} = K_i\_i_{circ-cl\_\beta\alpha} = K_i\_i_{circ-cl\_\beta\beta} = 0.$$

- Output control.
  One (1) P for the $2\alpha\beta\gamma$ output voltage amplitude $V^*_{out-cl} = [V_{out-cl\_d} \quad 0]^T$, with the $V^*_{out-cl\_d}$ of equation (6) [32, Equation (1)] with (7).

Adaptive Control System.

The adaptive control system consists of the following six (6) controllers, which are configured according to the definitions given in equations (13)-(15). These controllers utilize the Lyapunov-type energy terms $V_{e_o}(t) = \frac{1}{2}e_o^T e_o$ and $V_{e_i}(t) = \frac{1}{2}e_i^T e_i$. Moreover, all base disturbances Δ_{o_b} and Δ_{i_b} are computed based on the equations (1) and (3) in a stable state (zero first-time-derivatives), considering rated values from Table 3 and unitary parameter values (taking the known disturbance portion).

- Input Control.
  - One (1) APBC (13) for the $2\alpha\beta\gamma$ ACV Control, with:

$$\Delta_{o\_b\_V_{Cavg}} = -\frac{4P_{rated}}{9V^*_C} = -0.19, \; K_{o\_V_{Cavg}} = \frac{K_{i\_I_{in-cl}}}{15} = 0.67,$$
$$\Gamma_{o\_V_{Cavg}} = Diag[\frac{1}{(1+0.19^2)} \; \frac{1}{(1+10^2)}] = Diag[0.9649 \; 0.0099], \; \sigma_{o\_V_{Cavg}} = 1.$$

Preprints (www.preprints.org) | NOT PEER-REVIEWED | Posted: 3 August 2023 doi:10.20944/preprints202308.0302.v1

The output of this ACV controller is the input cluster line current amplitude direct component reference $I^*_{Lin-cl\_d}$. Therefore the inner loop input cluster line current amplitude reference is $I^*_{Lin-cl} = [I_{Lin-cl\_d} \quad 0]^T$, having the following controller:

– One (1) PBMRAC (15) for the $2\alpha\beta\gamma$ input cluster line current, and filtering a 2 KHz reference input noise:

$$A_{ri\_in} = B_{ri\_in} = \frac{2000}{20} I_2 = 100 I_2,$$
$$K_{i\_in} = K_{i\_I_{circ-cl}}(2\pi f_{in}) I_2 - A_{ri\_in} = (3141.6 - 100) I_2 = -3041.6 I_2,$$
$$\Delta_{i\_b\_in} = 3\sqrt{2} V_{in\_rated}[1 \quad 1]^T = 933.6[1 \quad 1]^T,\ \sigma_{i\_in} = I_2,$$
$$\Gamma_{i\_in} = Diag[\frac{16}{(1+16^2)} \frac{16}{(1+16^2)} \frac{16}{(1+16^2)} \frac{16}{(1+16^2)} \frac{933.6}{(1+933.6^2)} \frac{933.6}{(1+933.6^2)} \frac{16}{(1+16^2)} \frac{16}{(1+16^2)}]$$
$$= Diag[0.0623\ 0.0623\ 0.0623\ 0.0623\ 0.001\ 0.001\ 0.099\ 0.099].$$

- CCV Imbalance Control.

– One (1) APBC (13) for the $2\alpha\beta\gamma$ intra-CCV imbalance.

$$\Delta_{o\_b\_V_{Cintra}} = -\frac{\sqrt{2} V_{in\_rated} I_{cir\_rated}}{\sqrt{6} V^*_C}[1 \quad 1 \quad 1 \quad 1]^T = -4.23[1 \quad 1 \quad 1 \quad 1]^T,$$
$$K_{o\_V_{Cintra}} = \frac{K_{i\_I_{circ-cl}}}{15} I_4 = 0.67 I_4,\ \sigma_{o\_V_{Cavg}} = I_4,$$
$$\Gamma_{o\_V_{Cintra}} = Diag[\frac{1}{(1+10^2)} \frac{1}{(1+10^2)} \frac{1}{(1+4.23^2)} \frac{1}{(1+4.23^2)}] = Diag[0.001\ 0.001\ 0.053\ 0.053].$$

– One (1) APBC (13) for the $2\alpha\beta\gamma$ inter-CCV imbalance.

$$\Delta_{o\_b\_V_{Cinter}} = -[-\frac{\sqrt{2} V_{out\_rated} I_{cir\_rated}}{\sqrt{3} V^*_C} \frac{\sqrt{2} V_{out\_rated} I_{cir\_rated}}{\sqrt{3} V^*_C} \frac{\sqrt{2} V_{in\_rated} I_{cir\_rated}}{\sqrt{3} V^*_C} \frac{\sqrt{2} V_{in\_rated} I_{cir\_rated}}{\sqrt{3} V^*_C}]^T,$$
$$= [7.7 \quad -7.7 \quad -6 \quad -6]^T,$$
$$K_{o\_V_{Cinter}} = \frac{K_{i\_I_{circ-cl}}}{15} I_4 = 0.67 I_4,\ \sigma_{o\_V_{Cavg}} = I_4,$$
$$\Gamma_{o\_V_{Cinter}} = Diag[\frac{1}{(1+7.7^2)} \frac{1}{(1+7.7^2)} \frac{1}{(1+6^2)} \frac{1}{(1+6^2)}] = Diag[0.016\ 0.016\ 0.027\ 0.027].$$

The inner controller is designed as follows

– One (1) PBMRAC (15) for the $2\alpha\beta\gamma$ circulating cluster current, and filtering a 3.0 KHz reference input noise:

$$A_{ri\_circ-cl} = B_{ri\_circ-cl} = 2\pi \frac{3000}{20} I_4 = 942.5 I_4,$$
$$K_{i\_circ-cl} = K_{i\_I_{circ-cl}}(2\pi(2 f_{out}) I_4 - A_{ri\_circ-cl} = (9424.7 - 942.5) I_4 = -8482.3 I_4,$$
$$\Delta_{i\_b\_circ-cl} = 0\ \sigma_{i\_circ-cl} = 0, \Gamma_{i\_circ-cl} = \frac{10}{(1+10^2)} I_4 = 0.099 I_4.$$

- Output control.
One (1) P for the output voltage amplitude $V^*_{out-cl} = [V_{out-cl\_d} \quad 0]^T$, using the $V^*_{out-cl\_d}$ of equation (6) [32, Equation (1)] joined to (7).

The following sections present the comparative results of the M3C feeding the four PMSMs, each moving a centrifugal pump. The results were obtained with a simulation time of 8 s, under the following situations are described: normal operation, input phase imbalance, a cluster cell short-circuit, and an opened cluster cell.

For all cases, the set points in this $2\alpha\beta\gamma$ coordinate are: $V^*_{Cavg} = 3V^*_C = 4500V$, $V^*_{Cintra_{C_D}} = 0$, and $V^*_{Cinter} = 0$. Moreover, the reference rotor angular speed $\omega_{r\_rated}{}^* =$ is 0 rad/s between 0 s and 1 s, having a ramp up reaching ω_{r_rated} at 5 s and kept constant the remaining time.

4.1. Results Under a Normal Operation

Figure 3 shows the comparative results under a normal operation. Here, we operate with the rated input and output voltages.

Preprints (www.preprints.org) | NOT PEER-REVIEWED | Posted: 3 August 2023 doi:10.20944/preprints202308.0302.v1

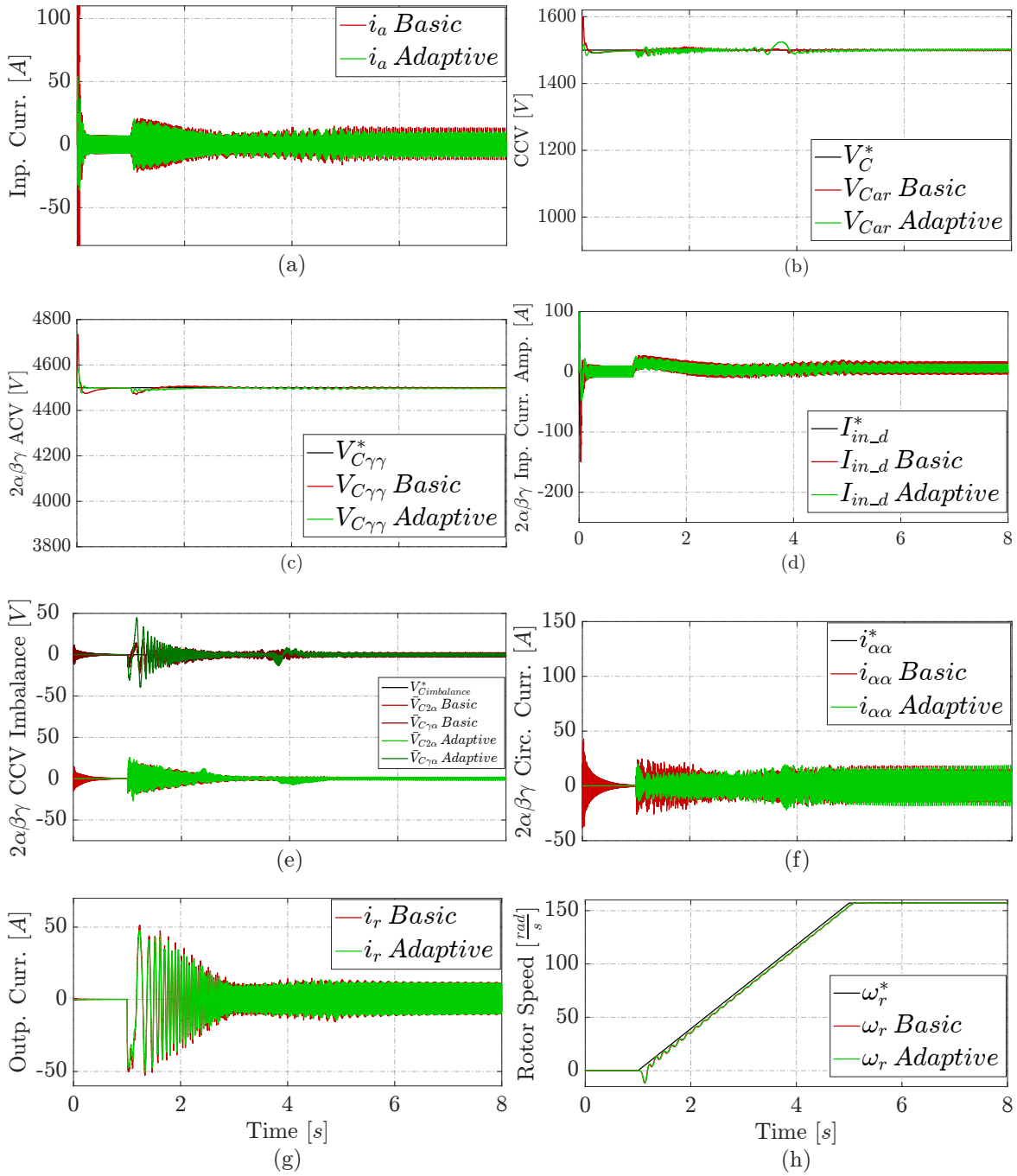

Figure 3. Comparative results under normal operation, (a) Phase a input current, (b) Branch ar CCV, (c) Controlled $2\alpha\beta\gamma$ ACV, (d) Controlled d component of the input current amplitude in $2\alpha\beta\gamma$, (e) Controlled intra and inter CCV imbalance in $2\alpha\beta\gamma$, (f) Controlled $\alpha\alpha$ component of the circulating current in $2\alpha\beta\gamma$, (g) Phase r output current, (h) PMSM angular rotor speed.

Figure 3 (a) and (g) demonstrate that the M3C adaptive proposal results in 25 % lower input and output current consumption (with a reduction of 5 A) compared to the basis control that utilizes PI controllers. Moreover, the adaptive controllers also exhibit less input current overshoot than the PI controllers.

Figure 3 (b) shows that the proposed M3C adaptive control has a 64 % less CCV overshoot (with a 70 V reduction) than the basic solution. Both adaptive and basic solutions ensure that the rotor speed follows the reference, as shown in Figure 3 (h).

Preprints (www.preprints.org) | NOT PEER-REVIEWED | Posted: 3 August 2023 doi:10.20944/preprints202308.0302.v1

Regarding the directly controlled variables in double-$\alpha\beta\gamma$ coordinates, both adaptive and basic solution also follow the reference. However, the adaptive solution has lower overshoots of ACV in Figure 3 (c), input current amplitude in Figure 3 (d), intra and inter CCV Imbalance in Figure 3 (e), circulating current in Figure 3 (f). Moreover the adaptive proposal consumes less input and circulation currents. As for the basic solution, the adaptive one has a 5 KHz noisy input amplitude in double-$\alpha\beta\gamma$.

4.2. Results Under an Input Phase Imbalance

Figure 4 displays the comparative results under an input phase imbalance. This first fault considers a drop of 10% of the "a" phase voltage, starting at 3 seconds.

Figure 4 (a) and (g) illustrates that prior to the fault, the M3C adaptive proposal results in 25 % lower input and output current consumption, with a reduction of 5 A compared to the basis control. The adaptive controllers also show less input current overshoot than the PI controllers. However, during the first second after the fault, the basic solution deteriorated while the adaptive approach recover its better performance faster.

Figure 4 (b) shows that the proposed M3C adaptive control has a 64 % less CCV overshoot (with a 70 V reduction) than the basic solution, similar to Figure 3 (b). However, the basic solution deteriorated after the fault while the adaptive approach tend to recover its performance.

Figure 4 (h) demonstrates that both the proposal and basic M3C controllers maintain the rotor speed in line with the reference, similar to Figure 3 (d). This is evident even when a fault occurs at the second 3, as it does not affect the pumping speed response.

Regarding the variables in double-$\alpha\beta\gamma$ coordinates; again, the adaptive solution has lower overshoots of ACV in Figure 3 (c), input current amplitude in Figure 3 (d), intra and inter CCV Imbalance in Figure 3 (e), circulating current in Figure 3 (f). Moreover, the adaptive proposal consumes less input and circulation currents before the fault. After the fault, the adaptive proposal completely recover its performance within 2 s in contrast to the basic solution.

Preprints (www.preprints.org) | NOT PEER-REVIEWED | Posted: 3 August 2023 doi:10.20944/preprints202308.0302.v1

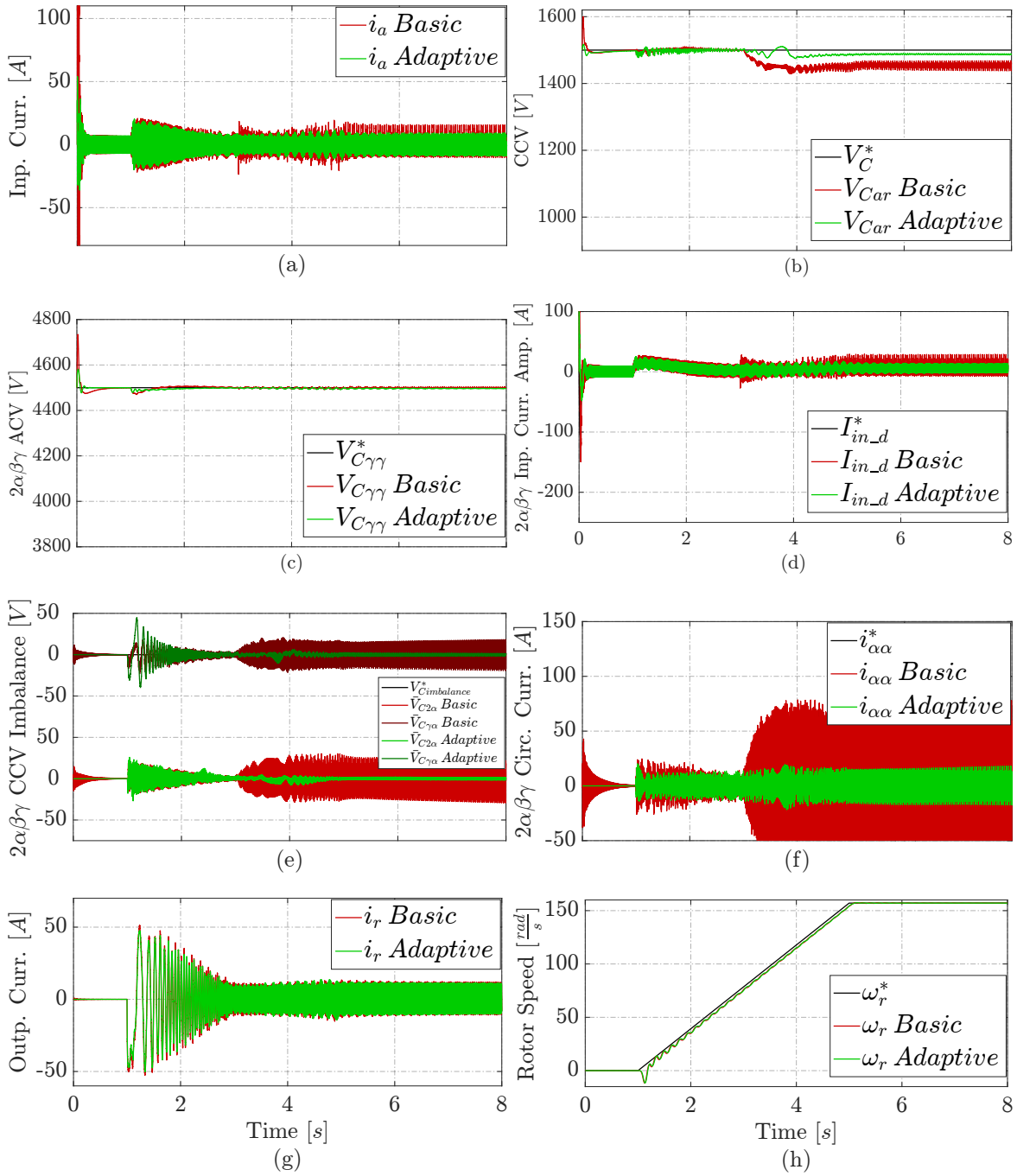

Figure 4. Comparative results under an input voltage imbalance, with a 10% voltage drop in phase *a* at 3 seconds, (a) Phase *a* input current, (b) Branch *ar* CCV, (c) Controlled $2\alpha\beta\gamma$ ACV, (d) Controlled *d* component of the input current amplitude in $2\alpha\beta\gamma$, (e) Controlled intra and inter CCV imbalance in $2\alpha\beta\gamma$, (f) Controlled $\alpha\alpha$ component of the circulating current in $2\alpha\beta\gamma$, (g) Phase *r* output current, (h) PMSM angular rotor speed.

4.3. Results Under a Cluster Cell Short Circuit

Figure 5 exhibits the comparative results under a cluster cell short circuit. This fault happens in cell one of the cluster *ar* at 3 seconds.

Preprints (www.preprints.org) | NOT PEER-REVIEWED | Posted: 3 August 2023 doi:10.20944/preprints202308.0302.v1

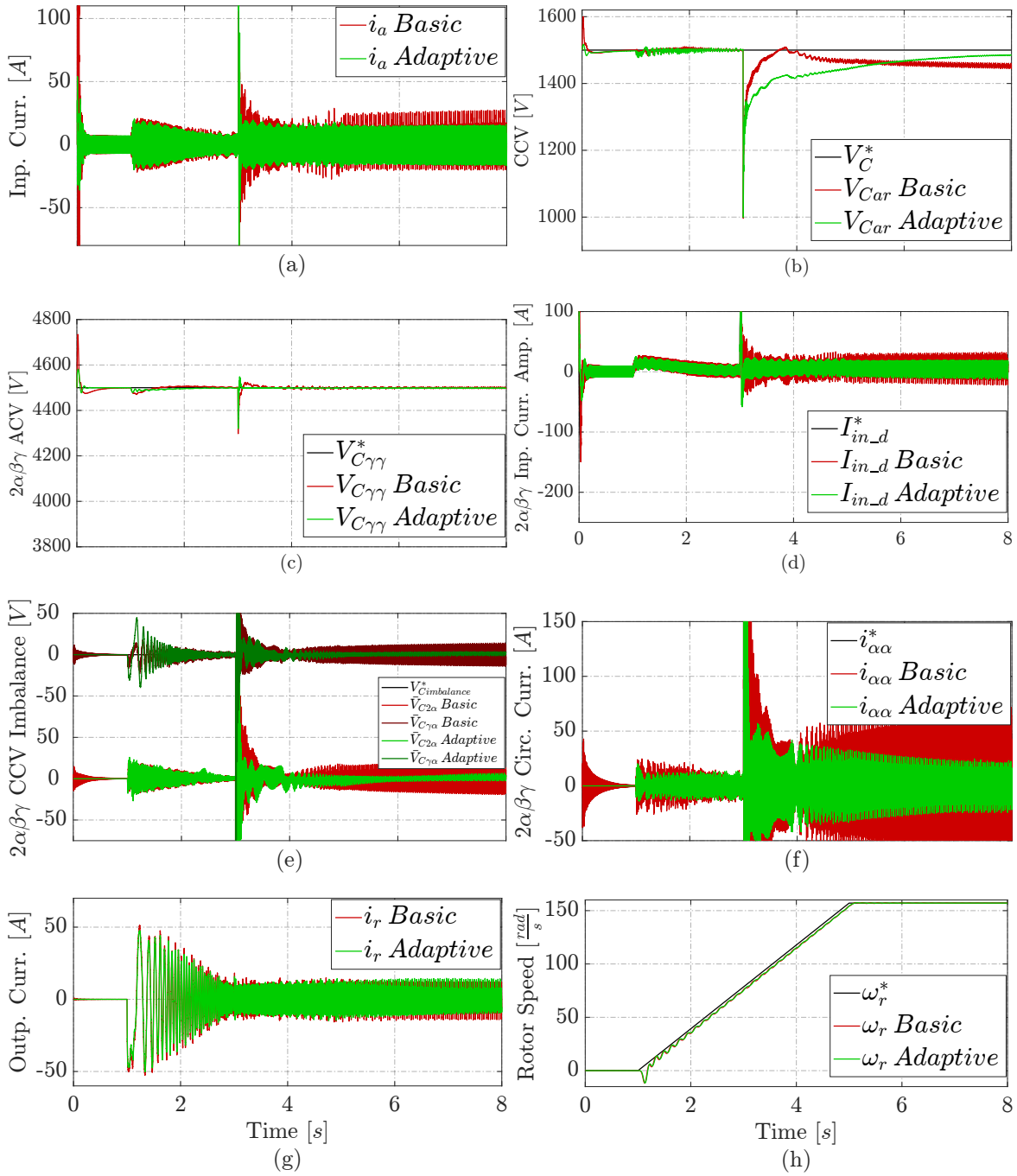

Figure 5. Comparative results under a cluster *ar* short circuit at 3 seconds, (a) Phase *a* input current, (b) Branch *ar* CCV, (c) Controlled $2\alpha\beta\gamma$ ACV, (d) Controlled *d* component of the input current amplitude in $2\alpha\beta\gamma$, (e) Controlled intra and inter CCV imbalance in $2\alpha\beta\gamma$, (f) Controlled $\alpha\alpha$ component of the circulating current in $2\alpha\beta\gamma$, (g) Phase *r* output current, (h) PMSM angular rotor speed.

Figure 5 (a) and (g) show that prior to the fault, the M3C adaptive proposal results in 25% lower input and output current consumption, with a reduction of 5 A compared to the basis control. However, during the first two seconds after the fault, the basic solution deteriorated and had a 70% increase in input current consumption, increasing by 35 A compared to the adaptive approach.

Figure 5 (b) shows that the M3C adaptive control method has a 64% reduction in CCV overshoot compared to the basic solution, reducing $70V$. This reduction is similar to the one shown in Figure 3 (b).

Preprints (www.preprints.org) | NOT PEER-REVIEWED | Posted: 3 August 2023 doi:10.20944/preprints202308.0302.v1

However, the basic solution demonstrates a quicker CCV to recovery after the fault tending towards the CCV reference of $1500V$.

Figure 5 (h) demonstrates that both the proposal and basic M3C controllers maintain the rotor speed in line with the reference, similar to Figures 3 (d) and 4 (d). Again. this is observed even after the fault happens at the second 3, which does not have an impact on the pumping speed's response.

Regarding the variables in double-$\alpha\beta\gamma$ coordinates; a similar behaviour than shown in 3 is obtained. The adaptive solution has lower overshoots of ACV in Figure 5 (c), input current amplitude in Figure 5 (d), intra and inter CCV Imbalance in Figure 5 (e), and circulating current in Figure 5 (f). After the fault, the adaptive solution completely recover its performance within 2 s; while the basic solution does not.

4.4. Results Under an Opened Cluster Cell

Figure 6 exhibits the comparative results under an opened cluster cell. This fault occurs in cell one of the cluster ar at 3 seconds.

Preprints (www.preprints.org) | NOT PEER-REVIEWED | Posted: 3 August 2023 doi:10.20944/preprints202308.0302.v1

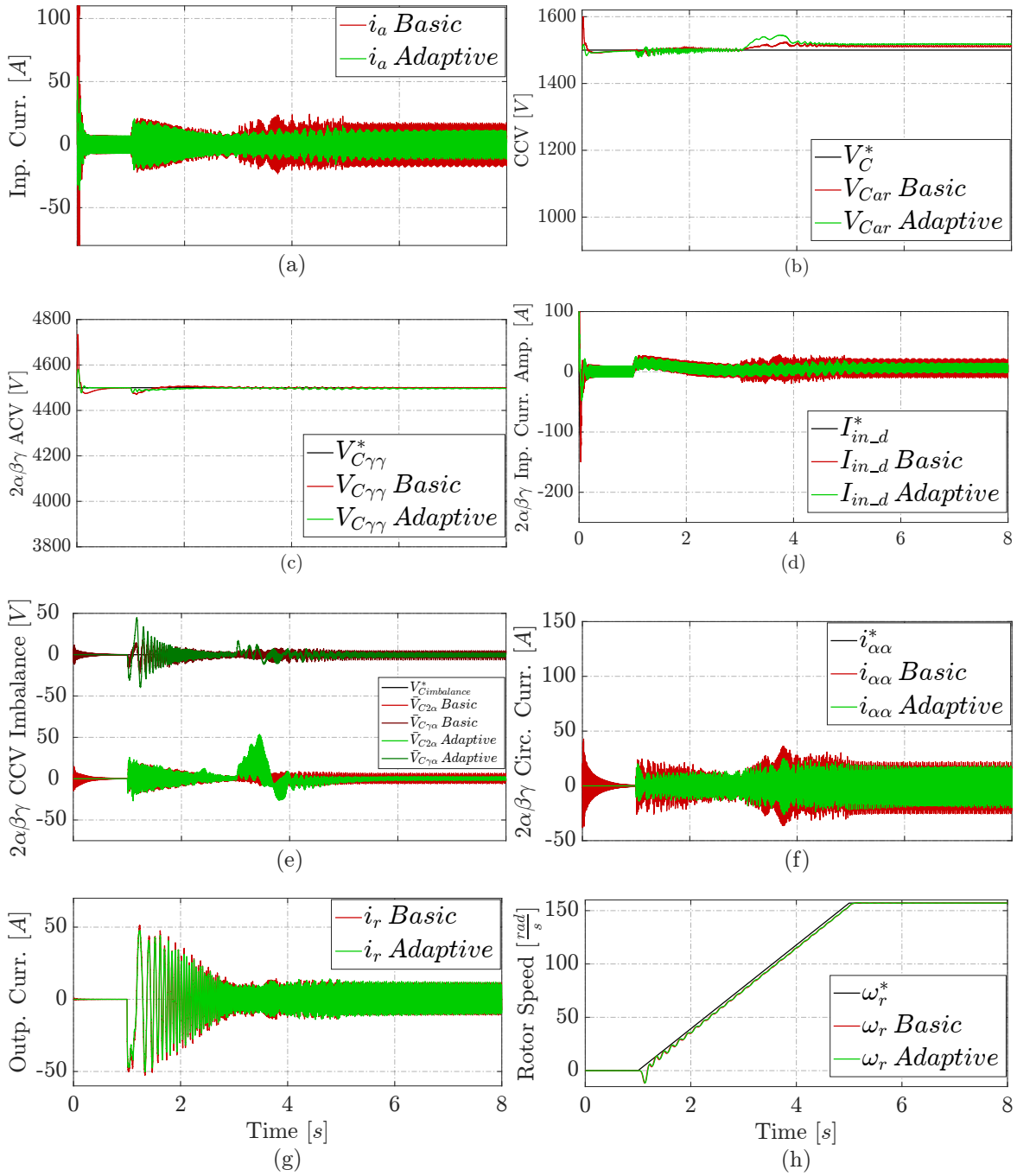

Figure 6. Comparative results under a cluster *ar* open circuit at 3 seconds, (a) Phase *a* input current, (b) Branch *ar* CCV, (c) Controlled $2\alpha\beta\gamma$ ACV, (d) Controlled *d* component of the input current amplitude in $2\alpha\beta\gamma$, (e) Controlled intra and inter CCV imbalance in $2\alpha\beta\gamma$, (f) Controlled $\alpha\alpha$ component of the circulating current in $2\alpha\beta\gamma$, (g) Phase *r* output current, (h) PMSM angular rotor speed.

Figure 6 describes a similar behaviour than in previously described faulty situations. However, both solutions have a lower degradation under this fault.

5. Conclusions

In this study, an adaptive control for an M3C-based variable speed drive powering multiple PMSM-driven centrifugal pumps was proposed. he study found that the adaptive proposal offers better performance and fault tolerance compared to the non-adaptive solution. The first step was

to obtain the multivariable M3C state-space model for control, which allowed for the design and implementation of novel MIMO adaptive controllers.

Notably, the paper proposed and applied a novel cascade APBC-PBMRAC to the M3C. Simulation results demonstrate that the proposal and basic M3C controllers ensure the rotor speed follows the reference, even when a fault occurs. However, the proposal has several advantages over the basic solution:

1. It reduces the number of non-adaptive PI controllers from thirteen (16) to five (5) MIMO adaptive controllers.
2. It is a more straightforward solution that does not require plant parameters knowledge, reducing commissioning time.
3. The proposed adaptive control has less overshoots than the basic solution.
4. Additionally, it shows a more stable CCV response (less noisy), as expected due to the APBC-PBMRAC design.
5. Finally, the basic solution tends to remain degraded after a fault, while the adaptive approach tends to recover quickly from any studied fault.

Author Contributions: Conceptualization, methodology, writing—original draft preparation, and visualization, R.M.-B. and J.C.T.-T.; investigation, formal analysis, supervision, project administration, data curation, and resources and funding acquisition, J.C.T.-T. and M.D.; validation, software, and writing—review and editing; R.M.-B. All authors have read and agreed to the published version of the manuscript.

Funding: This research was funded by FONDECYT Chile, grant 1220168; and FONDEQUIP Chile, grant EQM200234.

Institutional Review Board Statement: Not applicable.

Informed Consent Statement: Not applicable.

Data Availability Statement: Not applicable.

Acknowledgments: The Authors thank Abdiel Ricaldi-Morales for its technical support in the adaptive control implementation

Conflicts of Interest: The authors declare no conflict of interest.

Sample Availability: Not applicable.

Appendix A

This section starts by describing the M3C state-space dynamical model obtaining.

Appendix A.1. Inner control Loop M3C Dynamical model

The M3C inner loop dynamical model involves the following equation, obtained after applying Kirchhoff's voltage law to the power system of Figure 1 [22, Figure 2], [25] and rearranging terms in a matrix form (for details, please see Appendix A.3):

x-y Voltage-current model [6, Equation (9)]

$$v_{in-xy} = L\dot{i}_{cl-xy} + v_{cl-xy} + v_{out-xy} + v_{nN-xy}, \tag{A1}$$

Preprints (www.preprints.org) | NOT PEER-REVIEWED | Posted: 3 August 2023 doi:10.20944/preprints202308.0302.v1

where L is the coupling inductor inductance shown in Figure 1. Moreover, the instantaneous input phase voltage v_{in-xy}, cluster phase current i_{cl-xy}, cluster phase voltage v_{cl-xy}, output phase voltage v_{out-xy}, and neutral voltage v_{nN-xy} are defined as follows:

$$\begin{aligned} v_{in-xy} &= \begin{bmatrix} v_a & v_b & v_c \\ v_a & v_b & v_c \\ v_a & v_b & v_c \end{bmatrix}, \; i_{cl-xy} = \begin{bmatrix} i_{ar} & i_{br} & i_{cr} \\ i_{as} & i_{bs} & i_{cs} \\ i_{at} & i_{bt} & i_{ct} \end{bmatrix}, \; v_{cl-xy} = \begin{bmatrix} v_{ar} & v_{br} & v_{cr} \\ v_{as} & v_{bs} & v_{cs} \\ v_{at} & v_{bt} & v_{ct} \end{bmatrix}, \\ v_{out-xy} &= \begin{bmatrix} v_r & v_r & v_r \\ v_s & v_s & v_s \\ v_t & v_t & v_t \end{bmatrix}, \; v_{nN-xy} = \begin{bmatrix} 1 & 1 & 1 \\ 1 & 1 & 1 \\ 1 & 1 & 1 \end{bmatrix}, \end{aligned} \tag{A2}$$

where v_a, v_b, v_c are the instantaneous phase voltages of the power supply. The instantaneous phase cluster currents and voltages are i_{ar}, i_{br}, i_{cr}, i_{as}, i_{bs}, i_{cs}, i_{at}, i_{bt}, i_{ct} and v_{ar}, v_{br}, v_{cr}, v_{as}, v_{bs}, v_{cs}, v_{at}, v_{bt}, v_{ct} respectively. Finally, v_r, v_s, v_t are the instantaneous load phase voltages.

For independent control, a double-$\alpha\beta\gamma$ transformation $\mathcal{C}X\mathcal{C}^T$ [22] is applied to (A1). It consists in multiplying (A1) by the $\alpha\beta\gamma$ transform $\mathcal{C}$ [22] from the left and the right side, with matrix X representing each phase variable v_{in-xy}, i_{cl-xy}, v_{cl-xy}, v_{out-xy}, and v_{nN-xy}. As a result, we have:

Double-$\alpha\beta\gamma$ Voltage-current model [6, Equation (18)]

$$\sqrt{3}v_{in-2\alpha\beta\gamma} = L\dot{i}_{cl-2\alpha\beta\gamma} + v_{cl-2\alpha\beta\gamma} + \sqrt{3}v_{out-2\alpha\beta\gamma} + 3v_{nN-2\alpha\beta\gamma}, \tag{A3}$$

where the $\alpha\beta\gamma$ transform $\mathcal{C}$ [22], the input phase voltage $v_{in-2\alpha\beta\gamma}$, the cluster phase current $i_{cl-2\alpha\beta\gamma}$, the cluster phase voltage $v_{cl-2\alpha\beta\gamma}$, the output phase voltage $v_{out-2\alpha\beta\gamma}$, and the neutral voltage $v_{nN-2\alpha\beta\gamma}$ are following defined:

$$\begin{aligned} \mathcal{C} &= \begin{bmatrix} \frac{\sqrt{2}}{\sqrt{3}} & \frac{-\sqrt{2}}{2\sqrt{3}} & \frac{-\sqrt{2}}{2\sqrt{3}} \\ 0 & \frac{\sqrt{2}}{2} & \frac{-\sqrt{2}}{2} \\ \frac{\sqrt{3}}{3} & \frac{\sqrt{3}}{3} & \frac{\sqrt{3}}{3} \end{bmatrix}, \; v_{in-2\alpha\beta\gamma} = \begin{bmatrix} 0 & 0 & 0 \\ 0 & 0 & 0 \\ v_{in_\alpha} & v_{in_\beta} & v_{in_\gamma} \end{bmatrix}, \; i_{cl-2\alpha\beta\gamma} = \begin{bmatrix} i_{\alpha\alpha} & i_{\beta\alpha} & i_{\gamma\alpha} \\ i_{\alpha\beta} & i_{\beta\beta} & i_{\gamma\beta} \\ i_{\alpha\gamma} & i_{\beta\gamma} & i_{\gamma\gamma} \end{bmatrix}, \\ v_{cl-2\alpha\beta\gamma} &= \begin{bmatrix} v_{\alpha\alpha} & v_{\beta\alpha} & v_{\gamma\alpha} \\ v_{\alpha\beta} & v_{\beta\beta} & v_{\gamma\beta} \\ v_{\alpha\gamma} & v_{\beta\gamma} & v_{\gamma\gamma} \end{bmatrix}, \; v_{out-2\alpha\beta\gamma} = \begin{bmatrix} 0 & 0 & v_{out_\alpha} \\ 0 & 0 & v_{out_\beta} \\ 0 & 0 & v_{out_\gamma} \end{bmatrix}, \; v_{nN-2\alpha\beta\gamma} = \begin{bmatrix} 0 & 0 & 0 \\ 0 & 0 & 0 \\ 0 & 0 & 1 \end{bmatrix}. \end{aligned} \tag{A4}$$

Here, v_{in_α}, v_{in_β}, v_{in_γ} are the phase voltages of the power supply in double-$\alpha\beta\gamma$ coordinates. The cluster phase currents and phase voltages in double-$\alpha\beta\gamma$ coordinates are $i_{\alpha\alpha}$, $i_{\beta\alpha}$, $i_{\gamma\alpha}$, $i_{\alpha\beta}$, $i_{\beta\beta}$, $i_{\gamma\beta}$, $i_{\alpha\gamma}$, $i_{\beta\gamma}$, $i_{\gamma\gamma}$ and $v_{\alpha\alpha}$, $v_{\beta\alpha}$, $v_{\gamma\alpha}$, $v_{\alpha\beta}$, $v_{\beta\beta}$, $v_{\gamma\beta}$, $v_{\alpha\gamma}$, $v_{\beta\gamma}$, $v_{\gamma\gamma}$, respectively. Moreover, v_{out_α}, v_{out_β}, v_{out_γ} are the load phase voltages in double-$\alpha\beta\gamma$ coordinates.

Based on previous equations (A3) and (A4), the obtained decoupled state-space model for the input port, circulating currents, and output port is [25, Figure 2], [6, Figure 5]:

Double-$\alpha\beta\gamma$ State-space model of instantaneous voltage-current [6, Equations (19)–(21)]

$$\begin{aligned} \dot{i}_{in-cl} &= -\tfrac{1}{L}v_{in-cl} + \tfrac{\sqrt{3}}{L}v_{in}, && \text{Input phase current} \\ \dot{i}_{cir-cl} &= -\tfrac{1}{L}v_{cl}, && \text{Circulating phase current} \\ \dot{i}_{out-cl} &= -\tfrac{1}{L}v_{out-cl} - \tfrac{\sqrt{3}}{L}v_{out}, && \text{Output phase current} \end{aligned} \tag{A5}$$

with the instantaneous input phase voltage v_{in} having an input frequency ω_{in}, and the instantaneous output phase voltage v_{out} having an output frequency ω_{out}. These variables, joined the instantaneous

Preprints (www.preprints.org) | NOT PEER-REVIEWED | Posted: 3 August 2023 doi:10.20944/preprints202308.0302.v1

cluster phase currents i_{in-cl}, i_{cir-cl}, i_{out-cl}, and the instantaneous cluster voltages v_{in-cl}, v_{cl}, v_{out-cl}, are defined as:

$$\begin{aligned} i_{in-cl} &= \begin{bmatrix} i_{\alpha\gamma} \\ i_{\beta\gamma} \end{bmatrix}, v_{in} = \begin{bmatrix} v_{in_\alpha} \\ v_{in_\beta} \end{bmatrix}, v_{in-cl} = \begin{bmatrix} v_{\alpha\gamma} \\ v_{\beta\gamma} \end{bmatrix}, \\ i_{cir-cl} &= \begin{bmatrix} i_{\alpha\alpha} & i_{\beta\alpha} \\ i_{\alpha\beta} & i_{\beta\beta} \end{bmatrix}, v_{cl} = \begin{bmatrix} v_{\alpha\alpha} & v_{\beta\alpha} \\ v_{\alpha\beta} & v_{\beta\beta} \end{bmatrix}, \\ i_{out-cl} &= \begin{bmatrix} i_{\gamma\alpha} \\ i_{\gamma\beta} \end{bmatrix}, v_{out} = \begin{bmatrix} v_{out_\alpha} \\ v_{out_\beta} \end{bmatrix}, v_{out-cl} = \begin{bmatrix} v_{\gamma\alpha} \\ v_{\gamma\beta} \end{bmatrix}. \end{aligned} \tag{A6}$$

Finally, multiplying the Park Transformation P [24] from the left by the input and output phase current equations of (A5), these are converted to their dq coordinates to allow their amplitudes control. The circulating phase current equation of (A5) remains the same for the control of this instantaneous variable. Moreover, we consider the input cluster line current control, related to the phase current as $I_{Lin-cl} = \sqrt{3} I_{in-cl}$. As a result, the previous model (A5) takes the form:

Double-$\alpha\beta\gamma$ Voltage-current state-space model

$$\begin{aligned} \dot{I_{Lin-cl}} &= -\tfrac{\sqrt{3}}{L} V_{in-cl} + \tfrac{3}{L} V_{in}, && \text{Input phase current amplitude} \\ \dot{i_{cir-cl}} &= -\tfrac{1}{L} v_{cl}, && \text{Circulating phase current} \\ \dot{I_{out-cl}} &= -\tfrac{1}{L} V_{out-cl} - \tfrac{\sqrt{3}}{L} V_{out}, && \text{Output phase current amplitude} \end{aligned} \tag{A7}$$

where the Park Transformation P, the amplitudes of the input phase voltage V_{in}, output phase voltage V_{out}, cluster input line current I_{Lin-cl}, cluster output phase current I_{out-cl}, and cluster phase voltages V_{in-cl}, V_{out-cl}, all in d-q coordinates, are defined as:

$$\begin{aligned} P &= \begin{bmatrix} cos(\theta) & sin(\theta) \\ -sin(\theta) & cos(\theta) \end{bmatrix}, I_{Lin-cl} = \begin{bmatrix} I_{Lin-cl\_d} \\ I_{Lin-cl\_q} \end{bmatrix}, V_{in} = \begin{bmatrix} V_{in\_d} \\ V_{in\_q} \end{bmatrix}, \\ V_{in-cl} &= \begin{bmatrix} V_{in-cl\_d} \\ V_{in-cl\_q} \end{bmatrix}, I_{out-cl} = \begin{bmatrix} I_{out-cl\_d} \\ I_{out-cl\_q} \end{bmatrix}, V_{out} = \begin{bmatrix} V_{out\_d} \\ V_{out\_q} \end{bmatrix}, V_{out-cl} = \begin{bmatrix} V_{out-cl\_d} \\ V_{out-cl\_q} \end{bmatrix}, \end{aligned} \tag{A8}$$

where I_{Lin-cl_d} and I_{Lin-cl_q} are the amplitude components of the input coordinates of the cluster line currents. V_{in_d} and V_{in_q} are the amplitude components of the power supply phase voltage. V_{in-cl_d} and V_{in-cl_q} are the amplitude components of the input coordinates of the cluster phase voltages. I_{out-cl_d} and I_{out-cl_q} are the amplitude components of the output cluster phase currents. V_{out_d} and V_{out_q} are the amplitude components of the power supply phase voltage. Finally, V_{out-cl_d} and V_{out-cl_q} are the amplitude components of the output cluster phase voltages. The Park transformation uses $\theta = \theta_{in} = \int \omega_{in} d\tau$ for the input signals and $\theta = \theta_{out} = \int \omega_{out} d\tau$ for the output signals.

The following section describes the outer-loop M3C dynamical model obtaining.

Appendix A.2. Outer control Loop M3C Dynamical model

The outer loop M3C dynamical model considers the formula $I_C = C\dot{V}_{Cijk}$ of an ideal capacitor instantaneous current I_C, depending on the capacitance C and the capacitor voltage variation $\dot{V_{Cijk}}$ of a cell shown in Figure 1. Then, this last expression is re-expressed to obtain the variation rate of the cluster capacitor voltage $V_{Cij} = \sum_{k=1}^{3}(V_{Cijk})$ in terms of the power through a cluster P_{cl} as $\dot{V_{Cij}} = \frac{1}{CV_C} P_{cl}$ [22, Equation (8)]. Finally, applying this concept to the M3C, assuming the clusters have three cells (summing their voltage variation expressions), are balanced, and all capacitors are the same,

Preprints (www.preprints.org) | NOT PEER-REVIEWED | Posted: 3 August 2023 doi:10.20944/preprints202308.0302.v1

and that the average cluster capacitor voltage fluctuates $\epsilon(t)$ times around its required value V_C^*, the following matrix expression is obtained:

x-y Cluster capacitor voltage-power state-space model

$$\dot{V}_{C-xy} = \frac{1}{C\epsilon(t)V_C^*} P_{cl-xy}. \tag{A9}$$

The reference cluster capacitor voltage mean value is $V_C^* \geq 1.2 \cdot \sqrt{2} \cdot (V_{in\_rated} + V_{out\_rated})$, where V_C^* is a multiple of 3 (number of cells per cluster). Moreover, the instantaneous cluster capacitor voltage V_{C-xy} and cluster power P_{cl-xy} are defined as follows:

$$V_{C-xy} = \begin{bmatrix} V_{Car} & V_{Cbr} & V_{Ccr} \\ V_{Cas} & V_{Cbs} & V_{Ccs} \\ V_{Cat} & V_{Cbt} & V_{Cct} \end{bmatrix}, \; P_{cl-xy} = \begin{bmatrix} P_{ar} & P_{br} & P_{cr} \\ P_{as} & P_{bs} & P_{cs} \\ P_{at} & P_{bt} & P_{ct} \end{bmatrix}, \tag{A10}$$

where the cluster capacitor instantaneous voltages are V_{Car}, V_{Cbr}, V_{Ccr}, V_{Cas}, V_{Cbs}, V_{Ccs}, V_{Cat}, V_{Cbt}, V_{Cct}.

Again, for independent control, a double-$\alpha\beta\gamma$ transformation $\mathcal{C}X\mathcal{C}^T$ [22] is applied to (A9). Thus, (A9) is multiplied by the $\alpha\beta\gamma$ transform $\mathcal{C}$ [22] from the left and the right side, with matrix X representing the instantaneous cluster capacitor voltage V_{C-xy} and the cluster instantaneous power P_{cl-xy} (A10). Then, re-expressing the obtained result in a state space form, we have:

Double-$\alpha\beta\gamma$ state-space model of instantaneous voltage-power

$$\begin{array}{ll} \dot{V}_{Cavg} = \frac{1}{C\epsilon(t)V_C^*} P_{avg}, & \text{ACV} \\ \dot{V}_{Cintra} = \frac{1}{C\epsilon(t)V_C^*} P_{intra}, & \text{Intra-CCV imbalance} \\ \dot{V}_{Cinter} = \frac{1}{C\epsilon(t)V_C^*} P_{inter}, & \text{Inter-CCV imbalance} \end{array} \tag{A11}$$

having the following variables definitions:

$$\begin{aligned} V_{Cavg} &= V_{C\gamma\gamma}, \; P_{avg} = P_{\gamma\gamma}, \\ V_{Cintra} &= \begin{bmatrix} V_{C\alpha\alpha} & V_{C\alpha\beta} & V_{C\beta\alpha} & V_{C\gamma\alpha} \end{bmatrix}^T, P_{intra} = \begin{bmatrix} P_{\alpha\alpha} & P_{\alpha\beta} & P_{\beta\alpha} & P_{\gamma\alpha} \end{bmatrix}^T, \\ V_{Cinter} &= \begin{bmatrix} V_{C\alpha\gamma} & V_{C\beta\gamma} & V_{C\gamma\alpha} & V_{C\gamma\beta} \end{bmatrix}^T, P_{inter} = \begin{bmatrix} P_{\alpha\gamma} & P_{\beta\gamma} & P_{\gamma\alpha} & P_{\gamma\beta} \end{bmatrix}^T. \end{aligned} \tag{A12}$$

Here, in double-$\alpha\beta\gamma$ coordinates are $v_{C\alpha\alpha}$, the cluster capacitor instantaneous voltages components, $v_{C\beta\alpha}$, $v_{C\gamma\alpha}$, $v_{C\alpha\beta}$, $v_{C\beta\beta}$, $v_{C\gamma\beta}$, $v_{C\alpha\gamma}$, $v_{C\beta\gamma}$, $v_{C\gamma\gamma}$ and the instantaneous cluster power components are $P_{\alpha\alpha}$, $P_{\beta\alpha}$, $P_{\gamma\alpha}$, $P_{\alpha\beta}$, $P_{\beta\beta}$, $P_{\gamma\beta}$, $P_{\alpha\gamma}$, $P_{\beta\gamma}$, $P_{\gamma\gamma}$, which are clearly defined in [6, Equations (26)-(33)]. However, there is an issue with the intra-CCV and inter-CCV imbalance control. Every power component could be controlled by controlling certain component of the circulating current i_{cir-cl} (A6) but $P_{\gamma\alpha}$ [6, Equations (32)] that would be controlled by $i_{\alpha\alpha}$ as $P_{\alpha\gamma}$ [6, Equations (30)]. Therefore, an extra auxiliary transformation is made after multiplying from the left the intra-CCV imbalance equation of (A11) by the matrix C_D [25] as a solution to allow control. Moreover, the power formulas are re-expressed as a function of the phase voltages and phase currents as detailed in [6, Equations (38)-(45)] separating the control terms from the rest, which are considered as a disturbance. Finally, the state-space form for control takes the following form:

Double-$\alpha\beta\gamma$ voltage-power state-space model

Preprints (www.preprints.org) | NOT PEER-REVIEWED | Posted: 3 August 2023 doi:10.20944/preprints202308.0302.v1

$$\begin{aligned}
\dot{V}_{Cavg} &= \frac{V_{avg}(t)}{3C\epsilon(t)V_C^*} I_{Lin-cl_d} + \Delta_{avg}(t), && \text{ACV} \\
\dot{V}_{CintraD} &= \frac{V_{intra}(t)^T}{\sqrt{6}C\epsilon(t)V_C^*} T_r I_{cir1} + \Delta_{intra_{C_D}}(t), && \text{Intra-CCV imbalance} \\
\dot{V}_{Cinter} &= \frac{V_{inter}(t)^T}{\sqrt{3}C\epsilon(t)V_C^*} I_{cir2} + \Delta_{inter}(t), && \text{Inter-CCV imbalance}
\end{aligned} \tag{A13}$$

where the auxiliary transformation matrix C_D [25], capacitor voltage V_{Cintra}, V_{Cinter}, V_{Cavg}, the cluster voltage V_{intra}, V_{inter}, V_{avg}, the cluster current I_{cir1}, I_{cir2}, I_{avg}, and the disturbances Δ_{intra}, Δ_{inter}, Δ_{avg}, are following defined:

$$\begin{aligned}
C_D =& \frac{1}{2}\begin{bmatrix} 1 & 0 & 0 & 1 \\ 0 & 1 & -1 & 0 \\ 1 & 0 & 0 & -1 \\ 0 & 1 & 1 & 0 \end{bmatrix}, T_r = \begin{bmatrix} 0 & 0 & 1 & 0 \\ 0 & 0 & 0 & 1 \\ 1 & 0 & 0 & 0 \\ 0 & 1 & 0 & 0 \end{bmatrix}, \\
V_{avg} = V_{in_\alpha}, \quad V_{CintraD} =& C_D V_{Cintra} = \begin{bmatrix} V_{C1\alpha} & V_{C1\beta} & V_{C2\alpha} & V_{C2\beta} \end{bmatrix}^T, \\
V_{intra} =& \begin{bmatrix} V_{in_\alpha} & V_{in_\alpha} & V_{in_\alpha} & V_{in_\alpha} \end{bmatrix}^T, \\
V_{inter} =& \begin{bmatrix} -V_{out_\alpha} & V_{out_\alpha} & V_{in_\alpha} & V_{in_\alpha} \end{bmatrix}^T, \\
I_{cir1} =& \begin{bmatrix} I_{1\alpha_1} & I_{1\beta_1} & I_{2\alpha_1} & I_{2\beta_1} \end{bmatrix}^T, \\
I_{cir2} =& \begin{bmatrix} I_{1\alpha_2} & I_{1\beta_2} & I_{2\alpha_2} & I_{2\beta_2} \end{bmatrix}^T, \\
\Delta_{avg} = \Delta_{\gamma\gamma}, \quad \Delta_{intra_{C_D}} =& \begin{bmatrix} \Delta_{2\alpha} & \Delta_{2\beta} & \Delta_{1\alpha} & \Delta_{1\beta} \end{bmatrix}^T, \\
\Delta_{inter} =& \begin{bmatrix} \Delta_{\alpha\gamma} & \Delta_{\beta\gamma} & \Delta_{\gamma\alpha} & \Delta_{\gamma\beta} \end{bmatrix}^T,
\end{aligned} \tag{A14}$$

where the disturbance terms are obtained from the power expressions [6, Equations (38)-(45)], [22, Equations (17)-(25)], after separating the control terms components. The result gives:

$$\Delta_{\gamma\gamma} = \frac{1}{3}(V_{in_\beta} I_{in_\beta}) - \frac{1}{3}(V_{out_\alpha} I_{out\alpha} + V_{out_\beta} I_{out_\beta}). \tag{A15}$$

$$\begin{aligned}
\Delta_{1\alpha} =& \frac{1}{6}[(V_{in_\alpha} I_{out_\alpha} - V_{out_\alpha} I_{in_\alpha}) + (V_{in_\beta} I_{out_\beta} - V_{out_\beta} I_{in_\beta})] \\
&+ \frac{1}{\sqrt{6}}[(-V_{in_\beta} I_{2\beta}) + (-V_{out_\alpha} I_{2\alpha} + V_{out_\beta} I_{2\beta})] - V_n I_{1\alpha}, \\
\Delta_{1\beta} =& \frac{1}{6}[(V_{in_\alpha} I_{out_\beta} - V_{out_\beta} I_{in_\alpha}) - (V_{in_\beta} I_{out_\alpha} - V_{out_\alpha} I_{in_\beta})] \\
&+ \frac{1}{\sqrt{6}}[(V_{in_\beta} I_{2\alpha}) + (V_{out_\alpha} I_{2\beta} + V_{out_\beta} I_{2\alpha})] - V_n I_{1\beta}, \\
\Delta_{2\alpha} =& \frac{1}{6}[(V_{in_\beta} I_{out_\alpha} - V_{out_\alpha} I_{in_\beta}) - (V_{in_\beta} I_{out_\beta} - V_{out_\beta} I_{in_\beta})] \\
&+ \frac{1}{\sqrt{6}}[(V_{in_\beta} I_{1\beta}) + (-V_{out_\alpha} I_{1\alpha} + V_{out_\beta} I_{1\beta})] - V_n I_{2\alpha}, \\
\Delta_{2\beta} =& \frac{1}{6}[(V_{in_\beta} I_{out_\beta} - V_{out_\beta} I_{in_\beta}) + (V_{in_\beta} I_{out_\alpha} - V_{out_\alpha} I_{in_\beta})] \\
&+ \frac{1}{\sqrt{6}}[(-V_{in_\beta} I_{1\alpha}) + (V_{out_\alpha} I_{1\beta} + V_{out_\beta} I_{1\alpha})] - V_n I_{2\beta}.
\end{aligned} \tag{A16}$$

Preprints (www.preprints.org) | NOT PEER-REVIEWED | Posted: 3 August 2023 doi:10.20944/preprints202308.0302.v1

$$
\begin{aligned}
\Delta_{\alpha\gamma} &= \frac{1}{3\sqrt{2}}[(V_{in_\alpha} I_{in_\alpha} - V_{in_\beta} I_{in_\beta})] - \frac{1}{\sqrt{3}}[V_{out_\alpha}(I_{2\alpha}) + V_{out_\beta}(I_{1\beta} + I_{2\beta}) - V_n I_{in_\alpha}],\\
\Delta_{\beta\gamma} &= -\frac{1}{3\sqrt{2}}[(V_{in_\alpha} I_{in_\beta} + V_{in_\beta} I_{in_\alpha})] - \frac{1}{\sqrt{3}}[V_{out_\alpha}(I_{2\beta}) + V_{out_\beta}(I_{1\alpha} - I_{2\alpha}) - V_n I_{in_\beta}],\\
\Delta_{\gamma\alpha} &= -\frac{1}{3\sqrt{2}}[(V_{out_\alpha} I_{out_\alpha} - V_{out_\beta} I_{out_\beta})] + \frac{1}{\sqrt{3}}[V_{in_\alpha}(I_{1\alpha}) + V_{in_\beta}(-I_{1\beta} + I_{2\beta}) - V_n I_{out_\alpha}],\\
\Delta_{\gamma\beta} &= \frac{1}{3\sqrt{2}}[(V_{out_\alpha} I_{out_\beta} + V_{out_\beta} I_{out_\alpha})] + \frac{1}{\sqrt{3}}[V_{in_\alpha}(I_{1\beta}) + V_{in_\beta}(I_{1\alpha} - I_{2\alpha}) - V_n I_{out_\beta}].
\end{aligned}
\tag{A17}
$$

The following section details the different vector and matrix transformations made in the previous state-space model obtaining.

Appendix A.3. Vector and Matrix Transformation Details

This section details the vector and matrix used transformations, starting from the managing feedback signals block located at the right lower side of Figure 2. First, the vector of the cluster capacitor voltages V_{Cij} is obtained after summing the capacitor voltages $\sum_{k=1}^{3}(V_{ijk})$ per cell k inside each cluster as follows:

$$
\overbrace{\begin{bmatrix}
V_{Car1} & V_{Car2} & V_{Car3}\\
V_{Cbr1} & V_{Cbr2} & V_{Cbr3}\\
V_{Ccr1} & V_{Ccr2} & V_{Ccr3}\\
V_{Cas1} & V_{Cas2} & V_{Cas3}\\
V_{Cbs1} & V_{Cbs2} & V_{Cbs3}\\
V_{Ccs1} & V_{Ccs2} & V_{Ccs3}\\
V_{Cat1} & V_{Cat2} & V_{Cat3}\\
V_{Cbt1} & V_{Cbt2} & V_{Cbt3}\\
V_{Cct1} & V_{Cct2} & V_{Cct3}
\end{bmatrix}}^{V_{Cijk}}
\Rightarrow \sum_{k=1}^{3}(V_{Cijk}) =
\overbrace{\begin{bmatrix}
\sum_{k=1}^{3} V_{Cark}\\
\sum_{k=1}^{3} V_{Cbrk}\\
\sum_{k=1}^{3} V_{Ccrk}\\
\sum_{k=1}^{3} V_{Cask}\\
\sum_{k=1}^{3} V_{Cbsk}\\
\sum_{k=1}^{3} V_{Ccsk}\\
\sum_{k=1}^{3} V_{Catk}\\
\sum_{k=1}^{3} V_{Cbtk}\\
\sum_{k=1}^{3} V_{Cctk}
\end{bmatrix}}^{\sum_{k=1}^{3} V_{Cijk}}
=
\overbrace{\begin{bmatrix}
V_{Car}\\ V_{Cbr}\\ V_{Ccr}\\ V_{Cas}\\ V_{Cbs}\\ V_{Ccs}\\ V_{Cat}\\ V_{Cbt}\\ V_{Cct}
\end{bmatrix}}^{V_{Cij}}.
\tag{A18}
$$

Then, the following rearrangements R are made to convert vectors to the matrix form to allow implementation. It applies to the measurement vectors of the cluster currents i_{ij} and the cluster capacitor voltage V_{Cij}:

$$
\overbrace{\begin{bmatrix}
i_{ar}\\ i_{br}\\ i_{cr}\\ i_{as}\\ i_{bs}\\ i_{cs}\\ i_{at}\\ i_{bt}\\ i_{ct}
\end{bmatrix}}^{i_{ij}}
\Rightarrow R(i_{ij}) =
\overbrace{\begin{bmatrix}
i_{ar} & i_{br} & i_{cr}\\
i_{as} & i_{bs} & i_{cs}\\
i_{at} & i_{bt} & i_{ct}
\end{bmatrix}}^{i_{xy}},
\overbrace{\begin{bmatrix}
V_{Car}\\ V_{Cbr}\\ V_{Ccr}\\ V_{Cas}\\ V_{Cbs}\\ V_{Ccs}\\ V_{Cat}\\ V_{Cbt}\\ V_{Cct}
\end{bmatrix}}^{V_{Cij}}
\Rightarrow R(V_{Cij}) =
\overbrace{\begin{bmatrix}
V_{Car} & V_{Cbr} & V_{Ccr}\\
V_{Cas} & V_{Cbs} & V_{Ccs}\\
V_{Cat} & V_{Cbt} & V_{Cct}
\end{bmatrix}}^{V_{Cxy}}.
\tag{A19}
$$

Preprints (www.preprints.org) | NOT PEER-REVIEWED | Posted: 3 August 2023 doi:10.20944/preprints202308.0302.v1

The matrix X previously obtained results are double-$\alpha\beta\gamma$ transformed $\mathcal{C}X\mathcal{C}^T$ [22]. The right lower side of Figure 2 shows these operations, multiplying X by the $\alpha\beta\gamma$ transform $\mathcal{C}$ [22] from the left and right sides. Following, for $X = i_{ij}$ and $X = V_{Cij}$, it gives:

$$\overbrace{\begin{bmatrix} \frac{\sqrt{2}}{\sqrt{3}} & \frac{-\sqrt{2}}{2\sqrt{3}} & \frac{-\sqrt{2}}{2\sqrt{3}} \\ 0 & \frac{\sqrt{2}}{2} & \frac{-\sqrt{2}}{2} \\ \frac{\sqrt{3}}{3} & \frac{\sqrt{3}}{3} & \frac{\sqrt{3}}{3} \end{bmatrix}}^{\mathcal{C}} \cdot \overbrace{\begin{bmatrix} i_{ar} & i_{br} & i_{cr} \\ i_{as} & i_{bs} & i_{cs} \\ i_{at} & i_{bt} & i_{ct} \end{bmatrix}}^{i_{xy}} \cdot \overbrace{\begin{bmatrix} \frac{\sqrt{2}}{\sqrt{3}} & 0 & \frac{\sqrt{3}}{3} \\ \frac{-\sqrt{2}}{2\sqrt{3}} & \frac{\sqrt{2}}{2} & \frac{\sqrt{3}}{3} \\ \frac{-\sqrt{2}}{2\sqrt{3}} & \frac{-\sqrt{2}}{2} & \frac{\sqrt{3}}{3} \end{bmatrix}}^{\mathcal{C}^T} = \overbrace{\begin{bmatrix} i_{\alpha\alpha} & i_{\beta\alpha} & i_{\gamma\alpha} \\ i_{\alpha\beta} & i_{\beta\beta} & i_{\gamma\beta} \\ i_{\alpha\gamma} & i_{\beta\gamma} & i_{\gamma\gamma} \end{bmatrix}}^{i_{cl-2\alpha\beta\gamma}}, \tag{A20}$$

$$\overbrace{\begin{bmatrix} \frac{\sqrt{2}}{\sqrt{3}} & \frac{-\sqrt{2}}{2\sqrt{3}} & \frac{-\sqrt{2}}{2\sqrt{3}} \\ 0 & \frac{\sqrt{2}}{2} & \frac{-\sqrt{2}}{2} \\ \frac{\sqrt{3}}{3} & \frac{\sqrt{3}}{3} & \frac{\sqrt{3}}{3} \end{bmatrix}}^{\mathcal{C}} \cdot \overbrace{\begin{bmatrix} V_{Car} & V_{Cbr} & V_{Ccr} \\ V_{Cas} & V_{Cbs} & V_{Ccs} \\ V_{Cat} & V_{Cbt} & V_{Cct} \end{bmatrix}}^{V_{Cxy}} \cdot \overbrace{\begin{bmatrix} \frac{\sqrt{2}}{\sqrt{3}} & 0 & \frac{\sqrt{3}}{3} \\ \frac{-\sqrt{2}}{2\sqrt{3}} & \frac{\sqrt{2}}{2} & \frac{\sqrt{3}}{3} \\ \frac{-\sqrt{2}}{2\sqrt{3}} & \frac{-\sqrt{2}}{2} & \frac{\sqrt{3}}{3} \end{bmatrix}}^{\mathcal{C}^T} = \overbrace{\begin{bmatrix} V_{C\alpha\alpha} & V_{C\beta\alpha} & V_{C\gamma\alpha} \\ V_{C\alpha\beta} & V_{C\beta\beta} & V_{C\gamma\beta} \\ V_{C\alpha\gamma} & V_{C\beta\gamma} & V_{C\gamma\gamma} \end{bmatrix}}^{V_{C-2\alpha\beta\gamma}}. \tag{A21}$$

Moreover, there are other rearrangements R made to convert the matrix obtained in (A20) and (A21) to their vector form to allow implementation. The resulting vectors are demultiplexed in managing feedback signals block of Figure 2. It delivers the cluster instantaneous phase currents and capacitor voltages defined in (A6) and (A14) (i_{in-cl}, $i_{circ-cl}$, i_{out-cl}, and V_{Cintra}, V_{Cinter}, V_{Cavg}) as follows:

$$\overbrace{\begin{bmatrix} i_{\alpha\alpha} & i_{\beta\alpha} & i_{\gamma\alpha} \\ i_{\alpha\beta} & i_{\beta\beta} & i_{\gamma\beta} \\ i_{\alpha\gamma} & i_{\beta\gamma} & i_{\gamma\gamma} \end{bmatrix}}^{i_{cl-2\alpha\beta\gamma}} \Rightarrow R(i_{cl-2\alpha\beta\gamma}) = \begin{bmatrix} i_{\alpha\gamma} \\ i_{\beta\gamma} \\ i_{\alpha\alpha} \\ i_{\alpha\beta} \\ i_{\beta\alpha} \\ i_{\beta\beta} \\ i_{\gamma\alpha} \\ i_{\gamma\beta} \\ i_{\gamma\gamma} \end{bmatrix}, \overbrace{\begin{bmatrix} V_{C\alpha\alpha} & V_{C\beta\alpha} & V_{C\gamma\alpha} \\ V_{C\alpha\beta} & V_{C\beta\beta} & V_{C\gamma\beta} \\ V_{C\alpha\gamma} & V_{C\beta\gamma} & V_{C\gamma\gamma} \end{bmatrix}}^{V_{C-2\alpha\beta\gamma}} \Rightarrow R(V_{C-2\alpha\beta\gamma}) = \begin{bmatrix} V_{C\alpha\alpha} \\ V_{C\alpha\beta} \\ V_{C\beta\alpha} \\ V_{C\beta\beta} \\ V_{C\alpha\gamma} \\ V_{C\beta\gamma} \\ V_{C\gamma\alpha} \\ V_{C\gamma\alpha} \\ V_{C\gamma\gamma} \end{bmatrix}. \tag{A22}$$

Additionally, the cluster instantaneous capacitor voltage intra-components are multiplied by the matrix C_D [25]:

$$\overbrace{\frac{1}{2}\begin{bmatrix} 1 & 0 & 0 & 1 \\ 0 & 1 & -1 & 0 \\ 1 & 0 & 0 & -1 \\ 0 & 1 & 1 & 0 \end{bmatrix}}^{C_D} \overbrace{\begin{bmatrix} V_{C\alpha\alpha} \\ V_{C\alpha\beta} \\ V_{C\beta\alpha} \\ V_{C\beta\beta} \end{bmatrix}}^{V_{Cintra}} = \overbrace{\begin{bmatrix} V_{C\alpha\alpha} + V_{C\beta\beta} \\ V_{C\alpha\beta} - V_{C\beta\alpha} \\ V_{C\alpha\alpha} - V_{C\beta\beta} \\ V_{C\alpha\beta} + V_{C\beta\alpha} \end{bmatrix}}^{V_{Cintra_{C_D}}} = \overbrace{\begin{bmatrix} V_{C1\alpha} \\ V_{C1\beta} \\ V_{C2\alpha} \\ V_{C2\beta} \end{bmatrix}}^{V_{Cintra_{C_D}}}. \tag{A23}$$

The outer signals of the Intra-CCV imbalance control are located at the left-center side of Figure 2. These are multiplied by the T_r^{-1} matrix to obtain i_{cir1} to be sumed with i_{cir2}. The result is multiplied by the inverse matrix C_D^{-1} to obtain the circulating current i^*_{cir-cl} as follows:

$$\overbrace{\begin{bmatrix} i^*_{1\alpha1} \\ i^*_{1\beta1} \\ i^*_{2\alpha1} \\ i^*_{2\beta1} \end{bmatrix}}^{i^*_{cir1}} = \overbrace{\begin{bmatrix} 0 & 0 & 1 & 0 \\ 0 & 0 & 0 & 1 \\ 1 & 0 & 0 & 0 \\ 0 & 1 & 0 & 0 \end{bmatrix}}^{T_r^{-1}} \overbrace{\begin{bmatrix} i^*_{2\alpha1} \\ i^*_{2\beta1} \\ i^*_{1\alpha1} \\ i^*_{1\beta1} \end{bmatrix}}^{i^*_{cir1D}}, \overbrace{\begin{bmatrix} i^*_{1\alpha1} \\ i^*_{1\beta1} \\ i^*_{2\alpha1} \\ i^*_{2\beta1} \end{bmatrix}}^{i^*_{cir1}} + \overbrace{\begin{bmatrix} i^*_{1\alpha2} \\ i^*_{1\beta2} \\ i^*_{2\alpha2} \\ i^*_{2\beta2} \end{bmatrix}}^{i^*_{cir2}} = \overbrace{\begin{bmatrix} i^*_{1\alpha} \\ i^*_{1\beta} \\ i^*_{2\alpha} \\ i^*_{2\beta} \end{bmatrix}}^{i^*_{Cintra_{C_D}}}, \tag{A24}$$

Preprints (www.preprints.org) | NOT PEER-REVIEWED | Posted: 3 August 2023 doi:10.20944/preprints202308.0302.v1

$$\overbrace{\begin{bmatrix} i^*_{1\alpha}+i^*_{2\alpha} \\ i^*_{1\beta}+i^*_{2\beta} \\ -i^*_{1\beta}+i^*_{2\beta} \\ i^*_{1\alpha}-i^*_{2\alpha} \end{bmatrix}}^{i^*_{cir-cl}} = \overbrace{\begin{bmatrix} 1 & 0 & 1 & 0 \\ 0 & 1 & 0 & 1 \\ 0 & -1 & 0 & 1 \\ 1 & 0 & -1 & 0 \end{bmatrix}}^{C_D^{-1}} \overbrace{\begin{bmatrix} i^*_{1\alpha} \\ i^*_{1\beta} \\ i^*_{2\alpha} \\ i^*_{2\beta} \end{bmatrix}}^{i^*_{cir-clD}} = \overbrace{\begin{bmatrix} i^*_{\alpha\alpha} \\ i^*_{\alpha\beta} \\ i^*_{\beta\alpha} \\ i^*_{\beta\beta} \end{bmatrix}}^{i^*_{cir-cl}}. \tag{A25}$$

Later, the output signal of the controllers (V^*_{in-cl}, V^*_{cl}, V^*_{out-cl}) are multiplexed, considering $v^*_{\gamma\gamma} = 0$, and the obtained vector is rearrangement R in the following matrix form:

$$\begin{bmatrix} v^*_{\alpha\gamma} \\ v^*_{\beta\gamma} \\ v^*_{\alpha\alpha} \\ v^*_{\alpha\beta} \\ v^*_{\beta\alpha} \\ v^*_{\beta\beta} \\ v^*_{\gamma\alpha} \\ v^*_{\gamma\beta} \\ v^*_{\gamma\gamma} \end{bmatrix} \Rightarrow R = \overbrace{\begin{bmatrix} v^*_{\alpha\alpha} & v^*_{\beta\alpha} & v^*_{\gamma\alpha} \\ v^*_{\alpha\beta} & v^*_{\beta\beta} & v^*_{\gamma\beta} \\ v^*_{\alpha\gamma} & v^*_{\beta\gamma} & v^*_{\gamma\gamma} \end{bmatrix}}^{v^*_{cl-2\alpha\beta\gamma}}. \tag{A26}$$

The obtained matrix $X = v^*_{cl-2\alpha\beta\gamma}$ is then multiplied by the inverse $\alpha\beta\gamma$ transformation matrix $\mathcal{C}^{-1}$ [22] from the left and right sides, obtaining the required cluster voltage as follows:

$$\overbrace{\begin{bmatrix} \frac{\sqrt{2}}{\sqrt{3}} & 0 & \frac{\sqrt{3}}{3} \\ \frac{-\sqrt{2}}{2\sqrt{3}} & \frac{\sqrt{2}}{2} & \frac{\sqrt{3}}{3} \\ \frac{-\sqrt{2}}{2\sqrt{3}} & \frac{-\sqrt{2}}{2} & \frac{\sqrt{3}}{3} \end{bmatrix}}^{\mathcal{C}^{-1}} \cdot \overbrace{\begin{bmatrix} v^*_{\alpha\alpha} & v^*_{\beta\alpha} & v^*_{\gamma\alpha} \\ v^*_{\alpha\beta} & v^*_{\beta\beta} & v^*_{\gamma\beta} \\ v^*_{\alpha\gamma} & v^*_{\beta\gamma} & v^*_{\gamma\gamma} \end{bmatrix}}^{v^*_{cl-2\alpha\beta\gamma}} \cdot \overbrace{\begin{bmatrix} \frac{\sqrt{2}}{\sqrt{3}} & \frac{-\sqrt{2}}{2\sqrt{3}} & \frac{-\sqrt{2}}{2\sqrt{3}} \\ 0 & \frac{\sqrt{2}}{2} & \frac{-\sqrt{2}}{2} \\ \frac{\sqrt{3}}{3} & \frac{\sqrt{3}}{3} & \frac{\sqrt{3}}{3} \end{bmatrix}}^{\mathcal{C}^{-1^T}} = \overbrace{\begin{bmatrix} v^*_{ar} & v^*_{br} & v^*_{cr} \\ v^*_{as} & v^*_{bs} & v^*_{cs} \\ v^*_{at} & v^*_{bt} & v^*_{ct} \end{bmatrix}}^{v^*_{xy}}. \tag{A27}$$

A final rearrangement R is made to convert the obtained matrix to the required voltage vector form as follows:

$$\overbrace{\begin{bmatrix} v^*_{ar} & v^*_{br} & v^*_{cr} \\ v^*_{as} & v^*_{bs} & v^*_{cs} \\ v^*_{at} & v^*_{bt} & v^*_{ct} \end{bmatrix}}^{v^*_{xy}} \Rightarrow R(v^*_{xy}) = \overbrace{\begin{bmatrix} v^*_{ar} \\ v^*_{br} \\ v^*_{cr} \\ v^*_{as} \\ v^*_{bs} \\ v^*_{cs} \\ v^*_{at} \\ v^*_{bt} \\ v^*_{ct} \end{bmatrix}}^{v^*_{ij}}. \tag{A28}$$

References

1. Beck, M.; Sperlich, A.; Blank, R.; Meyer, E.; Binz, R.; Ernst, M. Increasing energy efficiency in water collection systems by submersible PMSM well pumps. *Water* **2018**, *10*, 1310.
2. Candelo-Zuluaga, C.; Riba, J.R.; Espinosa, A.G.; Blanch, P.T. Customized PMSM design and optimization methodology for water pumping applications. *IEEE Transactions on Energy Conversion* **2021**, *37*, 454–465.
3. Kashif, M.; Singh, B. Reduced-Sensor-Based Multistage Model Reference Adaptive Control of PV-Fed PMSM Drive for Water Pump. *IEEE Transactions on Industrial Electronics* **2022**, *70*, 3782–3792.
4. Kashif, M.; Singh, B. Modified Active-Power MRAS Based Adaptive Control with Reduced Sensors for PMSM Operated Solar Water Pump. *IEEE Transactions on Energy Conversion* **2022**.

5. Pires, V.F.; Cordeiro, A.; Foito, D.; Pires, A.J. Fault-tolerant multilevel converter to feed a switched reluctance machine. *Machines* **2022**, *10*, 35.
6. Diaz, M.; Cardenas, R.; Ibaceta, E.; Mora, A.; Urrutia, M.; Espinoza, M.; Rojas, F.; Wheeler, P. An Overview of Modelling Techniques and Control Strategies for Modular Multilevel Matrix Converters. *Energies* **2020**, *13*. doi:10.3390/en13184678.
7. Kucka, J.; Karwatzki, D.; Mertens, A. AC/AC modular multilevel converters in wind energy applications: Design considerations **2016**. pp. 1–10.
8. Miura, Y.; Mizutani, T.; Ito, M.; Ise, T. Modular multilevel matrix converter for low frequency AC transmission **2013**. pp. 1079–1084.
9. Bontemps, P.; Milovanovic, S.; Dujic, D. Performance analysis of energy balancing methods for matrix modular multilevel converters. *IEEE Transactions on Power Electronics* **2022**, *38*, 2910–2924.
10. Fan, B.; Wang, K.; Wheeler, P.; Gu, C.; Li, Y. An optimal full frequency control strategy for the modular multilevel matrix converter based on predictive control. *IEEE Transactions on Power Electronics* **2017**, *33*, 6608–6621.
11. Fan, B.; Wang, K.; Wheeler, P.; Gu, C.; Li, Y. A branch current reallocation based energy balancing strategy for the modular multilevel matrix converter operating around equal frequency. *IEEE Transactions on Power Electronics* **2017**, *33*, 1105–1117.
12. Kawamura, W.; Chen, K.L.; Hagiwara, M.; Akagi, H. A low-speed, high-torque motor drive using a modular multilevel cascade converter based on triple-star bridge cells (MMCC-TSBC). *IEEE Transactions on Industry Applications* **2015**, *51*, 3965–3974.
13. Wang, C.; Zheng, Z.; Wang, K.; Li, Y. Fault detection and tolerant control of IGBT open-circuit failures in modular multilevel matrix converters. *IEEE Journal of Emerging and Selected Topics in Power Electronics* **2022**, *10*, 6714–6727.
14. Wang, C.; Zheng, Z.; Wang, K.; Yang, B.; Zhou, P.; Li, Y. Analysis and control of modular multilevel matrix converters under branch fault conditions. *IEEE Transactions on Power Electronics* **2021**, *37*, 1682–1699.
15. Wang, C.; Zheng, Z.; Wang, K.; Li, Y. Submodule Fault-Tolerant Control of Modular Multilevel Matrix Converters With Adaptive Optimum Common-Mode Voltage Injection. *IEEE Transactions on Power Electronics* **2022**, *37*, 7548–7554.
16. Erickson, R.W.; Al-Naseem, O.A. A new family of matrix converters **2001**. *2*, 1515–1520.
17. Diaz, M.; Cardenas, R.; Espinoza, M.; Rojas, F.; Mora, A.; Clare, J.C.; Wheeler, P. Control of wind energy conversion systems based on the modular multilevel matrix converter. *IEEE Transactions on Industrial Electronics* **2017**, *64*, 8799–8810.
18. Diaz, M.; Cárdenas Dobson, R.; Ibaceta, E.; Mora, A.; Urrutia, M.; Espinoza, M.; Rojas, F.; Wheeler, P. An overview of applications of the modular multilevel matrix converter. *Energies* **2020**, *13*, 5546.
19. Guo, F.; Yu, J.; Ni, Q.; Zhang, Z.; Meng, J.; Wang, Y. Grid-forming control strategy for PMSG wind turbines connected to the low-frequency AC transmission system. *Energy Reports* **2023**, *9*, 1464–1472.
20. Bravo, P.; Pereda, J.; Merlin, M.M.; Neira, S.; Green, T.C.; Rojas, F. Modular Multilevel Matrix Converter as Solid State Transformer for Medium and High Voltage AC Substations. *IEEE Transactions on Power Delivery* **2022**, *37*, 5033–5043.
21. Mora, A.; Urrutia, M.; Cárdenas, R.; Angulo, A.; Espinoza, M.; Díaz, M.; Lezana, P. Model-predictive-control-based capacitor voltage balancing strategies for modular multilevel converters. *IEEE Transactions on Industrial Electronics* **2018**, *66*, 2432–2443.
22. Kawamura, W.; Hagiwara, M.; Akagi, H. Control and experiment of a modular multilevel cascade converter based on triple-star bridge cells. *IEEE Transactions on Industry Applications* **2014**, *50*, 3536–3548.
23. Diaz, M.; Cardenas, R.; Espinoza, M.; Hackl, C.M.; Rojas, F.; Clare, J.C.; Wheeler, P. Vector control of a modular multilevel matrix converter operating over the full output-frequency range. *IEEE Transactions on Industrial Electronics* **2018**, *66*, 5102–5114.
24. Park, R.H. Two-reaction theory of synchronous machines generalized method of analysis-part I. *Transactions of the American Institute of Electrical Engineers* **1929**, *48*, 716–727.
25. Kammerer, F.; Gommeringer, M.; Kolb, J.; Braun, M. Energy balancing of the modular multilevel matrix converter based on a new transformed arm power analysis. 2014 16th European Conference on Power Electronics and Applications. IEEE, 2014, pp. 1–10.

26. Kawamura, W.; Chiba, Y.; Akagi, H. A broad range of speed control of a permanent magnet synchronous motor driven by a modular multilevel TSBC converter. *IEEE Transactions on Industry Applications* **2017**, *53*, 3821–3830.
27. Gili, L.C.; Dias, J.C.; Lazzarin, T.B. Review, Challenges and Potential of AC/AC Matrix Converters CMC, MMMC, and M3C. *Energies* **2022**, *15*, 9421.
28. Fan, B.; Wang, K.; Wheeler, P.; Gu, C.; Li, Y. An optimal full frequency control strategy for the modular multilevel matrix converter based on predictive control. *IEEE Transactions on Power Electronics* **2017**, *33*, 6608–6621.
29. Duran, A.; Ibaceta, E.; Diaz, M.; Rojas, F.; Cardenas, R.; Chavez, H. Control of a modular multilevel matrix converter for unified power flow controller applications. *Energies* **2020**, *13*, 953.
30. Kawamura, W.; Hagiwara, M.; Akagi, H.; Tsukakoshi, M.; Nakamura, R.; Kodama, S. AC-Inductors design for a modular multilevel TSBC converter, and performance of a low-speed high-torque motor drive using the converter. *IEEE Transactions on Industry Applications* **2017**, *53*, 4718–4729.
31. Arias-Esquivel, Y.; Cardenas, R.; Urrutia, M.; Diaz, M.; Tarisciotti, L.; Clare, J.C. Continuous control set model predictive control of a modular multilevel converter for drive applications. *IEEE Transactions on Industrial Electronics* **2022**, *70*, 8723–8733.
32. Travieso-Torres, J.C.; Vilaragut-Llanes, M.; Costa-Montiel, Á.; Duarte-Mermoud, M.A.; Aguila-Camacho, N.; Contreras-Jara, C.; Álvarez-Gracia, A. New adaptive high starting torque scalar control scheme for induction motors based on passivity. *Energies* **2020**, *13*, 1276.
33. Zhang, Z.; Jin, Y.; Xu, Z. Modeling and Control of Modular Multilevel Matrix Converter for Low-Frequency AC Transmission. *Energies* **2023**, *16*, 3474.
34. Narendra, K.S.; Annaswamy, A.M. *Stable adaptive systems*; Courier Corporation, 2012.
35. Travieso-Torres, J.C.; Duarte-Mermoud, M.A.; Sepuleveda, D.I. Passivity-based control for stabilization, regulation and tracking purposes of a class of nonlinear systems. *International Journal of adaptive control and signal processing* **2007**, *21*, 582–602.
36. Travieso-Torres, J.C.; Ricaldi-Morales, A.; Véliz-Tejo, A.; Leiva-Silva, F. Robust Cascade MRAC for a Hybrid Grid-Connected Renewable Energy System. *Processes* **2023**, *11*, 1774.
37. Travieso-Torres, J.C.; Duarte-Mermoud, M.A.; Estrada, J.L. Tracking control of cascade systems based on passivity: the non-adaptive and adaptive cases. *ISA transactions* **2006**, *45*, 435–445.
38. Ogata, K.; others. *Modern control engineering*; Vol. 5, Prentice hall Upper Saddle River, NJ, 2010.
39. Clarke, E. *Circuit analysis of AC power systems: symmetrical and related components*; Vol. 1, Wiley, 1943.
40. Eugene, L.; Kevin, W.; Howe, D. Robust and adaptive control with aerospace applications. *England: Springer-Verlag London* **2013**.